

Repainting the colour-mass diagrams by unearthing the green mountain: dust-rich S0 galaxies in the colour-(galaxy stellar mass) diagram, and the colour-(black hole mass) relations for dust-poor versus dust-rich galaxies

Alister W. Graham¹★

¹ Centre for Astrophysics and Supercomputing, Swinburne University of Technology, Hawthorn, VIC 3122, Australia

Accepted XXX. Received YYY; in original form ZZZ

ABSTRACT

Lenticular galaxies are notoriously misclassified as elliptical galaxies and, as such, a (disc inclination)-dependent correction for dust is often not applied to the magnitudes of dusty lenticular galaxies. This results in overly red galaxy colours, impacting their distribution in the colour-magnitude diagram. It is revealed how this has led to an underpopulation of the ‘green valley’ by hiding a ‘green mountain’ of massive dust-rich lenticular galaxies—known to be built from gas-rich major mergers—within the ‘red sequence’ of colour-(stellar mass) diagrams. Correcting for dust, a ‘green mountain’ appears at $M_{*,\text{gal}} \sim 10^{11} M_{\odot}$, along with signs of an extension to lower masses producing a ‘green range’ or ‘green ridge’ on the green side of the ‘red sequence’ and ‘blue cloud.’ The ‘red sequence’ is shown to be comprised of two components: a red plateau defined by elliptical galaxies with a near-constant colour and by lower-mass dust-poor lenticular galaxies, which are mostly a primordial population but may include faded/transformed spiral galaxies. The presence of the quasi-triangular-shaped galaxy evolution sequence, previously called the ‘Triangal’, is revealed in the galaxy colour-(stellar mass) diagram. It tracks the speciation of galaxies and their associated migration through the diagram. The connection of the ‘Triangal’ to previous galaxy morphology sequences (Fork, Trident, Comb) is also shown herein. Finally, the colour-(black hole mass) diagram is revisited, revealing how the dust correction generates a blue-green sequence for the spiral *and* dust-rich lenticular galaxies that is offset from a green-red sequence defined by the dust-poor lenticular and elliptical galaxies.

Key words: galaxies: bulges – galaxies: elliptical and lenticular, cD – galaxies: structure – galaxies: interactions – galaxies: evolution – (galaxies:) quasars: supermassive black holes

1 INTRODUCTION

Galaxy speciation, i.e., the evolution of galaxies from one type to another, tracks, among other things, the uni-directional growth of their central black hole¹ mass, M_{bh} , and bulge/spheroid stellar mass, $M_{*,\text{sph}}$. Galaxy-merger-induced jumps from one type of galaxy to another was initially observed (Graham 2012; Graham & Scott 2013; Scott et al. 2013) in the $M_{\text{bh}}-M_{*,\text{sph}}$ diagram due to the appearance of merger-built galaxies with cores depleted of stars

following a different trend to those without such central deficits.² Others have subsequently confirmed this scenario, including Kormendy & Ho (2013, their Section 6.7) and Saglia et al. (2016). Today, a more complete picture of these transitions is emerging, revealing transitions from spiral (S) to dust-rich lenticular (S0: e.g., Barnes & Hernquist 1996; Robertson & Bullock 2008) and from dust-rich S0 to either elliptical (ES)³ or elliptical (E) galaxies (Hernquist 1993), as described in Graham (2023c) and referred to as

★ E-mail: AGraham@swin.edu.au

¹ For massive black holes, ‘Hawking radiation’ (Hawking 1974, 1975; Zel’dovich 1976)—first discussed by Vladimir Gribov and Yakov Zel’dovich in 1972–1973 (Ansel’m et al. 1998; Dokshitzer 1998; Lipatov 1999; Azimov 2016)—tends to be dramatically outpaced by black hole accretions and mergers.

² This galaxy divide at around $2 \times 10^{11} M_{\odot}$ is discussed in Graham & Guzmán (2003), while the history of black hole scaling relations up to and including this separation of galaxy type is extensively reviewed in Graham (2016).

³ Liller (1966) introduced the ES notation to capture something of a halfway station between E and (massive) S0 galaxies. The term ‘ellicular’ was introduced/preferred (Graham et al. 2016) over ‘lenticular’ given that the

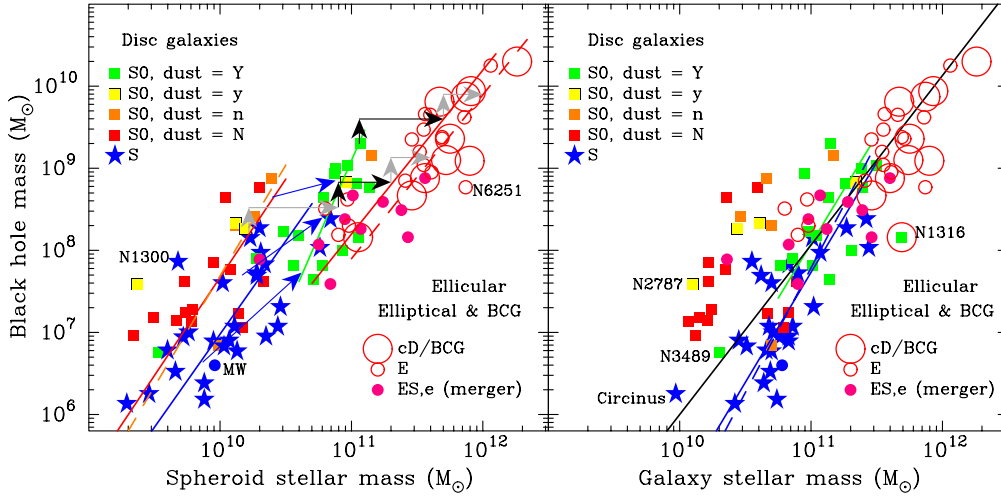


Figure 1. Adaption of figures 1 and A4 from [Graham \(2023c\)](#). Left panel: From left to right, the red (and dashed orange) line pertains to the dust=(n)O S0 galaxies (and when additionally including the dust=(n)nucleus-only S0 galaxies), while the other line colours are for the S (blue), S0 with dust=(Y)es-strong (green), and E plus ES,e (red) galaxies. The dashed red line is representative of the BCG. The grey and black arrows denote growth from major (equal mass) dry mergers, while the blue arrows denote growth from major gas-rich mergers. Right panel: The solid (and dashed) blue line corresponds to the S galaxies (after excluding Circinus). The green line pertains to S0 galaxies with dust=Y. (Arguably, the S and dust-rich S0 galaxies define a common sequence, and they have been combined in the CM_{bhd} (Section 4.3); many of the dust-rich S0 galaxies have mild levels of star formation ([Graham et al. 2023](#)); see also [Yi et al. \(2005\)](#).) The black line pertains to the cD/BCG, E, ES,e and dust=Y S0 galaxies and effectively represents the major-merger built galaxies. Slopes are around 2 to 3, with equations and details given in [Graham \(2023c\)](#).

‘punctuated equilibrium’ by [Graham & Sahu \(2023a\)](#). For convenience, these galaxy transitions are illustrated in Fig. 1, emerging from the (galaxy morphology)-aware $M_{\text{bh}}-M_{*,\text{sph}}$ diagram shown there. All common types of galaxies are now considered, and previous reasons for excluding significant numbers of galaxies are eliminated. These reasons included not following a nearly linear $M_{\text{bh}}-M_{*,\text{sph}}$ relationship due to an ‘over-massive black hole’ monster, having a suspected pseudobulge (regardless of the presence of a classical bulge) or being a merger remnant, and so on ([Kormendy & Ho 2013](#)). A more inclusive and unified scheme is rewriting our understanding of the coevolution of galaxies and their massive black holes.

The ubiquitous nature of massive black holes in regular galaxies was realised three decades ago (e.g., [Haehnelt & Rees 1993](#)) and has been supported by a continual stream of observations (e.g., [Tanaka et al. 1995](#); [Miyoshi et al. 1995](#); [Genzel et al. 1996, 1997](#); [Ghez et al. 1998](#); [Schödel et al. 2002](#); [Event Horizon Telescope Collaboration et al. 2019](#)). As black hole masses increase, so does their entropy ([Bekenstein 1973](#)). A spheroid’s stellar mass reflects its galaxy’s orbital entropy⁴, a proxy for disorder and chaos over ordered disc orbits. It is a measure of the dispersion of the orbital energy into more configurations, better filling the spherical volume or halo enclosing a galaxy. This greater appreciation of spheroid-building mergers and the coevolution of their central black hole helped solve a century-long mystery of galaxy evolution, giving

ES galaxy sample seemed more akin to E than S0 galaxies, with disc-to-total ratios generally less than 15 per cent ([Graham & Sahu 2023b](#)).

⁴ This remark excludes the entropy of suspected dark matter halos of non-baryonic matter ([Olive et al. 1981](#); [Fukuda et al. 1999](#)), including gravitinos ([Rarita & Schwinger 1941](#); [Grisaru et al. 1977](#); [Bond et al. 1982](#); [Pagels & Primack 1982](#)) and potential primordial low- and intermediate-mass black holes ([Hawking 1971](#); [Carr & Hawking 1974](#); [Carr & Kühnel 2020](#)) missed by gravitational lensing surveys (e.g., [Alcock et al. 2000](#); [Tisserand et al. 2007](#)) because they are either too small or too few, respectively.

rise to a reworked ‘Tuning Fork’ diagram ([Jeans 1928](#); [Hubble 1936](#)) referred to as the ‘Triangal’ and shown in Fig. 2.

Among its successes, the ‘Triangal’ has helped better link the Milky Way with the extragalactic population ([Graham 2023c](#)). Building on the Tuning Fork, the ‘Triangal’ strikes a new note by including evolutionary pathways due to acquisitions and mergers and involving a more extensive array of galaxy types, including elliptical galaxies and two or three varieties of S0 galaxies. There are the dust-rich S0 galaxies built from gas-rich, aka ‘wet’, mergers involving S galaxies (already polluted/fertilised with dust) (e.g., [Barnes & Hernquist 1996](#); [Bassett et al. 2017](#); [Rathore et al. 2022](#)), and the dust-poor S0 galaxies comprised of (some) faded S galaxies ([Gunn & Gott 1972](#); [Barr et al. 2007](#)) and (mostly) primordial S0 galaxies, which can have old, metal-poor stellar populations (e.g., [Rakos & Schombert 2004](#); [Marcum et al. 2004](#); [Paudel et al. 2010](#)) and low bulge-to-total (B/T) stellar mass ratios. The latter population need not all be old, though, and they might be better regarded as the first generation/incarnation of a galaxy, in which gas cooled sufficiently to contract into a disc (or ring) to allow star formation. They need never have possessed a spiral pattern. Those S0 galaxies that formed in the young Universe and did not transform their morphology could be thought of as today’s ‘ancients’ or ‘elders’ ([Lisker et al. 2006](#); [Sil’chenko 2013](#)). Those which formed at later times or experienced replenishment/rejuvenation ([Mapelli 2015](#); [Mapelli et al. 2015](#); [Rathore et al. 2022](#)) of their stellar ranks will appear younger, while local gas-dominated ‘dark galaxies’ may represent current-epoch counterparts (e.g., [Carignan & Freeman 1988](#); [Kennicutt & Skillman 2001](#)).

The ‘Triangal’ not only encapsulates the joint development of galaxies and black holes and has breathed life (clear evolutionary pathways) into past sequences of galaxy morphology (Fig. 2), but also applies to interpreting the (star formation rate: SFR)-(stellar mass) diagram ([Graham et al. 2023](#)). The current paper provides two additional applications of the ‘Triangal’. First, its presence

and operation are revealed in the galaxy colour-(stellar mass) diagram (CMD: e.g., Baum 1959; de Vaucouleurs 1961; Visvanathan & Sandage 1977; Sandage & Visvanathan 1978b; Kodama & Arimoto 1997; Martin et al. 2007; Schiminovich et al. 2007; Wyder et al. 2007). It must be noted that this paper benefits from countless prior works, and a sincere effort to acknowledge some of this relevant and interesting history is presented in Section 2 before the data for the present investigation is described in Section 3.

The CMD is often touted as a tool for the wholesale study of the extragalactic constituents of the cosmos. Nowadays, the CMD is typically considered to have three main features: a ‘red sequence’, ‘green valley’ (e.g., Martin et al. 2007; Salim 2014, and references therein) or ‘green plain’ (Quilley & de Lapparent 2022), and ‘blue cloud’. In Section 4, with attention to a greater range of galaxy types and using dust corrections for both late-type galaxies (LTGs) and early-type galaxies (ETGs) with dust-rich discs, the ‘green valley/plain’ is somewhat replaced by a ‘green mountain’ at $M_{*,\text{gal}} \sim 10^{11} M_{\odot}$ (Yi et al. 2005; Eales et al. 2018b; Graham et al. 2023), with an extension to lower masses forming what might be termed a ‘green range’ or ‘green ridge’. This extension was previously highlighted by Schweizer & Seitzer (1992) as due to a population later referred to as blue ETGs (e.g., Lisker et al. 2006; Driver et al. 2007b; Kannappan et al. 2009). In addition, a ‘red plateau’ or flat ‘dead sequence’⁵ (Romeo et al. 2008; Jiménez et al. 2011) at the high-mass end of the ‘red sequence’ is observed and shown to be defined by the (pure) E galaxies (Quilley & de Lapparent 2022), with the dust-poor S0 galaxies defining the sloped segment of the ‘red sequence’. These somewhat known but often missed elements of, and clues in, the CMD are evident here due to the refined galaxy morphologies. This engenders a better understanding of galaxy evolution than can be gleaned from using just an LTG versus ETG distinction.

Indeed, some motivation for investigating the CMD stems from recent developments in galaxy morphology studies. In particular, from the realisation that the dust morphology, and likely dust content⁶, of S0 galaxies, tracks their origin (Graham 2023b). This revelation into dust-poor and dust-rich S0 galaxies is likely also tied to the previously unexplained dual population of (low- and high-mass) S0 galaxies detected by van den Bergh (1990). Furthermore, it also incorporates the findings of Schweizer & Seitzer (1992) and Wegner & Grogin (2008), which revealed that ETGs with blue colours, relative to the ‘red sequence’, display signs of merger activity leading to star formation and thus a reduced mean age and more blue colour. Applying this knowledge to the CMD lends to additional growth trajectories beyond LTGs in the ‘blue cloud’ turning into red spirals (Spitzer & Baade 1951; Gunn & Gott 1972) or (low mass) discs transforming into ETGs (Farouki & Shapiro 1981; Moore et al. 1996), or LTG collisions directly (under ideal collisions) producing E galaxies (e.g., Roos & Norman 1979; Gerhard 1981; Negroponte & White 1983). Moreover, the analysis herein rewrites the description from Schawinski et al. (2014) for populating the ‘green valley’. Rather than S galaxy mergers rapidly quenching the star formation to produce red galaxies, these merger remnants tend to have persistent star formation (Graham et al. 2023) and are found here to linger at the green end of the ‘blue cloud’.

⁵ The term ‘dead sequence’ is not preferred because galaxies on the sloped ‘red sequence’ are also dead in the sense that they are not forming stars.

⁶ The dust-to-gas ratio is understandably higher in merger-built S0 galaxies than in S galaxies (Engelbracht et al. 2008; Baes et al. 2014).

Section 4.3 presents the second application of the ‘Triangal’, revealing its presence in the colour-(black hole mass) diagram (CM_{bb}D). Relations for dust-poor and dust-rich galaxies are established. Section 5 provides an extended discussion, while Section 6 summarises the main points.

2 GREATER CONTEXT SETTING: HISTORICAL DEVELOPMENTS

While this section can be skipped, it provides a fuller introduction to galaxy morphology, which some readers may appreciate. With what is now a relatively comprehensive schema for galaxy speciation, it seemed apt to review several relevant aspects as to how we got here. This section helps to place ideas and developments into a broader context than typically garnered, thereby providing a deeper understanding of the generations of work leading to studies of the CMD. It is mentioned when different galaxy types were recognised, as are past efforts to connect them via speculated morphological changes. References are provided to works by many pioneers upon whose shoulders we now stand. This section then segues to relevant notes regarding the measurement of galaxy colours.

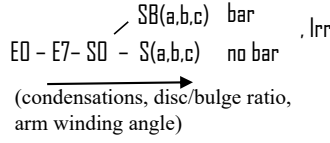
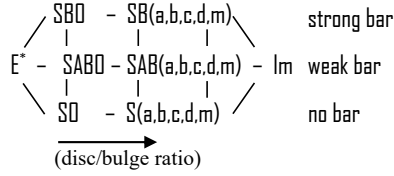
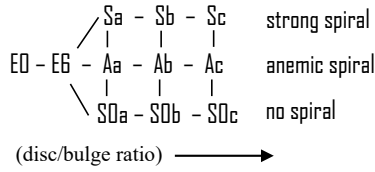
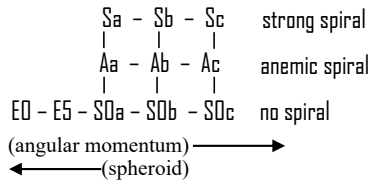
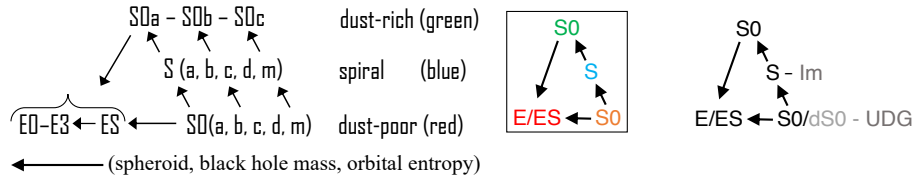
2.1 Galaxy Morphology

In the late 1700s and the first half of the 1800s, the Herschel family did not call out any spiral nebula, and their ~2500-member catalogues of nebulae and clusters of stars identified none as such (Herschel 1786, 1789, 1802). It was not until Lord William Parsons, the Right Honourable Third Earl of Rosse, built what was then the world’s largest (72-inch) telescope⁷ at Birr Castle, Ireland, that a spiral pattern was identified (Rosse 1850).⁸ Soon after, and perhaps for the first time, Alexander (1852) introduced the term ‘elliptical’ to distinguish elliptical-shaped nebulae from the newly-found spiral nebula. John Herschel’s General Catalogue of Nebulae and Clusters of Stars (Herschel 1864) subsequently called out five spiral nebulae among its ~5,000 entries, which additionally included planetary nebula and globular clusters of stars. The New General Catalogue (NGC: Dreyer 1888) was an expanded compilation that contained thousands of entries. While it also identified (only the same five) 2- and 3-branched spiral nebulae, including the ‘magnificent spiral’ in M51 reported by Rosse (1850), at that time, no nebulae were identified explicitly as lenticular or lenticular in shape. This was also true for the subsequent Index Catalogues (Dreyer 1895, 1910). However, with the application of photography to astronomy (Draper 1882; Huggins 1882; Common 1883), much deeper images could be acquired (Roberts 1893, 1895), and thus, fainter nebulae were discovered, and greater detail was observed in those already found.

While Reynolds (1920a,b) mentions ‘spindle’-shaped objects, which were thought to be edge-on spiral nebulae, Reynolds (1925) introduced examples of lenticular nebulae that are lens-like or lenticular in shape. These objects were identified explicitly as the suspected

⁷ At odds with John Herschel, William Parsons was of the view that the ‘nebular hypothesis’ for forming planets around stars (Swedenborg 1734; Kant 1755; Laplace 1796, 1825) was not the whole story and that many nebulae were, in fact, comprised of countless stars. His telescope was, in part, built to test this.

⁸ An additional 256 non-stellar objects were discovered (Parsons 1861, 1878) and would later be subsumed into the New General Catalogue (Dreyer 1888).

1925 – 1936 Tuning Forkde Vaucouleurs 1959 Barrelvan den Bergh 1976 RDDO TridentCappellari et al. 2011 ATLAS^{3D} CombGraham 2023 TriangalContributions

Alexander 1852 (angular momenta)
 Curtis 1918 (barred/non-barred, p.12)
 Jeans 1919 (E-to-S scheme from nebular hypothesis)
 Reynolds (1920a, spiral condensation sequence)
 Reynolds 1925 (S0 type, p.1016).
 Lundmark 1925, 1927 (classification schemes)
 Hubble 1926 (classification, early-to-late type)
 Reynolds 1927 (S0, arm winding, disc/bulge ratio)
 Jeans 1928 (Y-shaped tuning fork, Chapter XIII)
 Hubble 1936 (tuning fork diagram, p.45)

de Vaucouleurs 1959 (rings vs spirals gave 2nd axis to barrel. E* captures E, E+, S0⁰, S0⁺ types)

Vorontsov-Vel'Yaminov & Arkhipova 1962-1974 (catalogue of interacting galaxy classifications)

Spitzer & Baade (1951) proposed an S0 series of form paralleling the Sa, Sb, Sc galaxies

Liller 1966 (ES galaxies between E and S0 are fast-inner and slow-outer rotators)

Fall 1983 (angular momentum)
 Shaya & Tully 1984 (angular momentum)
 Elmegreen & Elmegreen 1987 (arm classifications)
 Bender 1988 (angular momentum)
 de Vaucouleurs et al. 1991 (catalogue)
 Capaccioli & Caon 1992 (angular momentum)
 Kormendy & Bender 1996 (classification scheme)

Buta et al. 2015 (CVRHS system and catalogue)
 Graham 2019 (Galaxy Grid including ES galaxies)

Figure 2. The accretion/merger-driven transitions to new morphological types — shown by the ‘Triangal’ (Graham 2023c) — are evident in Fig. 1 and track increases in a galaxy’s spheroid (aka bulge) and black hole mass. The transitions reveal the dust-rich S0 galaxies built from wet major mergers as a different population to the lower-mass dust-poor S0 galaxies, perhaps better regarded as ‘first generation’ galaxies rather than just ‘primordials’, thereby encapsulating delayed creation at later epochs. The transitions also show S galaxies (and Magellanic-like Irregular galaxies: Im) developed from accretions and gravitational perturbations of previously spiral-less disc galaxies. Major mergers of S0 galaxies build the ES and E galaxies. The extended schema, including dwarf S0 galaxies and ultra-diffuse galaxies (UDGs) in the lower right, shall be addressed in a forthcoming paper. Notes: RDDO = Revised David Dunlap Observatory. CVRHS system = Comprehensive de Vaucouleurs revised Hubble-Sandage (CVRHS) system. The location of disc galaxies with (i) weak vs. strong spiral arms, (ii) weak vs. strong bars, and (iii) ring/spiral variety (de Vaucouleurs 1959) in this accretion/merger-driven evolutionary schema will be explored in forthcoming work. References: (Alexander 1852; Curtis 1918; Jeans 1919; Reynolds 1920a; Lundmark 1925; Reynolds 1925; Hubble 1926; Lundmark 1927; Reynolds 1927; Jeans 1928; Hubble 1936; de Vaucouleurs 1959; Vorontsov-Vel’Yaminov & Arkhipova 1962; Liller 1966; Vorontsov-Vel’Yaminov & Arkhipova 1974; van den Bergh 1976; Fall 1983; Shaya & Tully 1984; Elmegreen & Elmegreen 1987; Bender 1988; de Vaucouleurs et al. 1991; Capaccioli & Caon 1992; Kormendy & Bender 1996; Cappellari et al. 2011; Buta et al. 2015; Graham 2019b, 2023c).

bridging population in the E to S evolutionary sequence of Jeans (1919), largely based on the ‘nebular hypothesis’ debated by J. Herschel and W. Parsons. The theory proposed that elliptical-shaped nebulae evolved into spiral-shaped nebulae by spinning-out material aided by passing encounters (Alexander 1852; Toomre & Toomre 1972). Hence, the origin of the early- and late-type galaxy nomenclature used today.

Extrapolating upon the numbers of new nebulae seen in pho-

tographed regions of the sky using the 8-inch Bache Doublet telescope at the Harvard College Observatory, Pickering (1890), with the aid of Mrs Williamina P. S. Fleming, estimated an increase of 50-60 per cent over the 7,840 nebulae in the NGC. Keeler (1899) later revealed there was far more to the cosmos than ever realised before when he estimated there were over 120,000 nebulae that would be seen if the sky was mapped with one-hour exposures using the Crossley 36-inch reflector (Keeler 1900). Perrine (1904)

subsequently estimated a figure of 500,000 to one million, and over the decades, this number has increased from nearly a billion through photographic work (e.g., [Lundmark 1956](#)) to 100-200 billion that are bright enough to be seen in the observable portion of the Universe by the *Hubble Space Telescope* ([Illingworth et al. 2013](#)), to a suspected two trillion ([Conselice et al. 2016](#)) with $M_* > 10^6 M_\odot$ out to $z = 8$. Due to galaxy mergers, these numbers can decline over time as the Universe matures according to the evolving galaxy merger rate ([Conselice et al. 2016](#)).

The question all this is leading to is, how do all these galaxies and galaxy types fit together? What clues may galaxy morphology (and colour) tell us about their origin? Galaxy classification schemes are an important first step in addressing this, and several have been put forward over the years (see [Graham 2019b](#), for a review). However, the challenging next step has been deciphering the correct evolutionary pathways between the different galaxy morphologies. A solution materialises in Fig. 1, taken from [Graham \(2023c\)](#), and it is pertinent to ask if and how the transitions seen there appear in the CMD. This requires the addition of key morphological information into the CMD beyond simply LTG versus ETG, and this is done here. The CMD is investigated for signatures of how galactic metamorphism may play out. To date, usually only the faded S galaxy and S galaxy merger origin are considered for S0 galaxies (e.g., [Deeley et al. 2020](#); [Coccatto et al. 2022](#)). Although, [Saha & Cortesi \(2018\)](#) explored the fragmentation of unstable discs at high- z , bypassing the spiral galaxy phase and leading to clumps that build up the bulge.

As for some of the better-known morphological classification schemes, Fig. 2 provides a summary of how the ‘Tuning Fork’ — displaying what is arguably still the most widely shown sequence of galaxy morphologies — has evolved over the last century to become the ‘Triangal’ ([Graham 2023c](#)), with evolutionary pathways and a new/key differentiation of lenticular galaxy type. This has revealed the initially unexpected, but with hindsight, obvious, bridging nature of LTGs between dust-poor and dust-rich S0 galaxies. Skimming the schemas in Fig. 2, it may be tempting to conclude that the ES galaxies ([Liller 1966](#)) are E4 to E7 galaxies, but this is not the case. The elongated E4 to E7 galaxies are invariably misclassified S0 galaxies (as noted by, for example, [Gorbachev 1970](#); [Michard 1984](#)), while the ES galaxies contain intermediate-scale discs that do not dominate the light at large radii, as is the case in S0 galaxies. The subtype ES,e galaxies are akin to elliptical galaxies and are likely built from dry major mergers of S0 galaxies that did not fully erase the disc component. Some of Liller’s ES galaxies have been labelled ‘disc ellipticals’ ([Nieto et al. 1988](#)), and they are simultaneously fast and slow rotators depending on the sampled aperture size ([Arnold et al. 2011](#); [Graham et al. 2017](#); [Bellstedt et al. 2017](#)). They are also identified as S0⁻ sp/E5-E7 type galaxies in the scheme of [Buta et al. \(2015, their table 1\)](#). Advancing this work, [Graham \(2023b\)](#) suggests that the more compact ES,b galaxies (aka ‘red nuggets’: [Daddi et al. 2005](#); [Damjanov et al. 2009](#)) might have formed from more ancient mergers involving gas-rich galaxies from the high-mass end of what are today’s dust-poor S0 galaxies. The ES,b galaxies may have bypassed the S galaxy phase of evolution. They appear more akin to high-density bulges than low-density elliptical galaxies, hence the introduced subscripts ‘b’ and ‘e’ on Liller’s ES notation.⁹

⁹ Perhaps ES,b galaxies would be better called ‘lentical’, and ‘ellicular’ reserved for the ES,e galaxies.

2.2 Colouring in the CMD

When [Hubble \(1936\)](#) presented what has come to be known as the Tuning Fork diagram — a rotated form of the [Jeans \(1928\)](#) Y-shaped diagram, as noted by [Hart & Berendzen \(1971, their footnote 42\)](#) and [van den Bergh \(1997\)](#) — he recognised that a galaxy’s colour correlated with its morphology, such that ETGs are red and LTGs are blue. It was subsequently realised that dwarf ETGs are bluer than giant ETGs (e.g., [Baum 1959](#); [de Vaucouleurs 1961](#); [Sandage & Visvanathan 1978b](#)), collectively forming the ‘red sequence’ of ETGs seen in colour-(absolute magnitude) or colour-(stellar mass) diagrams ([de Vaucouleurs 1961](#); [de Vaucouleurs & de Vaucouleurs 1972](#)). This sequence flattens, and the colours stabilise at both high masses (e.g., [Tremonti et al. 2004](#); [Jiménez et al. 2011](#)) and low masses (e.g., [de Vaucouleurs & Ables 1968, their figure 3](#)); see also [Roediger et al. \(2017, their figure 10\)](#).¹⁰ In contrast, the LTGs do not display a strong trend in the colour-magnitude diagram ([de Vaucouleurs & de Vaucouleurs 1972](#)), resulting in their so-called ‘blue cloud’.¹¹

Well after the eventual fall from grace (by the mid-1920s) of the ‘nebular hypothesis’, [Spitzer & Baade \(1951\)](#) still regarded the transitional galaxy population between S and E galaxies as S0 galaxies. However, they suggested this may occur from gas removal from, and the subsequent fading and reddening of, S galaxies. They speculated that a collision of two S galaxies would be such that the stellar components would pass through each other relatively unscathed. At the same time, the much higher number density of the gas particles would result in encounters that leave the gas behind at the collision site.¹² However, this idea tends to fail in the field environment because the stars and gas merge into a single galaxy, and it is not applicable in galaxy clusters where the encounter speeds are favourably higher but it is instead the cluster’s hot halo of gas that washes out a galaxy’s cold gas ([Gunn & Gott 1972](#); [Davies & Lewis 1973](#)), as can an array of alternate fast-acting processes (e.g., [Tanaka et al. 2004](#); [Aragón-Salamanca et al. 2006](#); [Rizzo et al. 2018](#); [Wright et al. 2019](#)).

While rapid dust-removal, from, say, ‘ram-pressure stripping’ ([Gunn & Gott 1972](#)), might initially act to make a galaxy bluer, the associated gas-removal and the ensuing passive fading from stellar evolution will soon redden a spiral galaxy and might result in the loss of the spiral pattern (e.g., [Smail et al. 2001](#); [Bekki et al. 2002](#); [Lisker et al. 2006](#); [Boselli et al. 2008](#); [Rathore et al. 2022](#)). The S galaxies can also slowly fade due to the gradual depletion of gas associated with star formation (e.g., [Barr et al. 2007](#); [Lilly et al. 2013](#)). However, the notion that *all* S0 galaxies are faded S galaxies was ruled out by the existence of S0 galaxies with higher masses than spiral galaxies ([Burstein et al. 2005](#)). That notion implicitly presupposes that spiral galaxies are primordial rather than having formed from pre-existing disc-dominated S0 galaxies.

The ‘Triangal’ takes the view that primordial star-forming S0 galaxies have faded to become the $z = 0$ dust-poor S0 galaxies; that is, there is no assumption that they were once S galaxies. Further-

¹⁰ At these low masses, $M_{*,\text{gal}} \lesssim 10^7 M_\odot$, the scatter in colour appears to become quite unwieldy, and the sequence disappears in some works (e.g., [Conselice 2002, their figure 1](#)).

¹¹ Interestingly, some of the galaxy magnitudes and morphologies obtained in Australia by Gérard and Antoinette de Vaucouleurs came from the 30-inch Reynolds’ telescope, which had been donated by Reynolds in 1924 to what would become Mount Stromlo Observatory ([Maddison 2011](#)).

¹² This phenomenon was also invoked to explain the Bullet Cluster ([Randall et al. 2008](#)).

more, while the passive evolution and fading of an S galaxy would change its colour from blue to red and therefore be associated with an upward movement in the CMD from the ‘blue cloud’ to the ‘red sequence’, the fading scenario encounters opposition when examining the $M_{\text{bh}}-M_{*,\text{gal}}$ diagram. This is because the fading scenario, in which the gas is gone and $M_{*,\text{gal}}$ does not change greatly¹³, would require M_{bh} to grow by an order of magnitude if faded S galaxies become dust-poor S0 galaxies (see Fig. 1). A related challenge for the fading S galaxy scenario is to grow the $M_{\text{bh}}/M_{*,\text{sph}}$ ratio by a factor of a few to match the $M_{\text{bh}}-M_{*,\text{sph}}$ relations for S and dust-poor S0 galaxies.

It is well known that, due to the relatively quick demise of massive hot blue stars and the longevity of less massive red stars, the mean colour of a stellar population reddens as it ages. This reddening occurs even in the presence of an exponentially declining star formation rate (Schmidt 1959). However, other factors are at play besides colour-changing stellar evolution as stars progress through the Hertzsprung-Russell (HR: Hertzsprung 1911; Russell 1914) diagram (e.g., Park & Lee 1997). For example, higher metallicity alters the initial mass function (IMF: Salpeter 1955; Tanvir & Krumholz 2023) of stars and retards the escape of energy from stars. The metals in a star increase the opacity and thus the internal pressure (thereby reducing the required luminosity and effective temperature to balance gravity), which makes them appear redder. In contrast, metal-poor stars are more blue.

An additional factor that is not intrinsic to the colours of a stellar population is the dust clouds that screen/filter the light before it reaches us, scattering the blue light and making the conglomerate of stellar blackbody spectra from a galaxy appear redder than it is. Corrections for Galactic extinction (through sightlines out of our galaxy) are readily applied using infrared-based dust extinction maps (Schlegel et al. 1998; Schlafly & Finkbeiner 2011). Empirical corrections for dust internal to external galaxies have been made from knowledge of the inclination of their disc to our line of sight (Driver et al. 2008). This also includes a correction for dust when the external discs are viewed face-on. Roughly half of a spiral galaxy’s bulge light at blue wavelengths, coming from the far side of a face-on galaxy, does not reach us. Because of the central concentration of dust, bulge light is more obscured than disc light. Given the trend of increasing bulge-to-disc, B/D , ratio with the galaxy mass, external dust corrections have the effect of making the slight slope to the ‘blue cloud’ less steep; that is, when applied, this dust correction is such that galaxies with higher B/D ratios become more blue than those with smaller B/D ratios.

Refined measurements have brought better recognition of a bridging population of galaxies in the CMD’s so-called ‘green valley’.¹⁴ Some of these ‘green valley’ galaxies have been identified as disturbed S0 galaxies (Schweizer & Seitzer 1992), and some were also identified as star-forming (Roediger et al. 2017, their figure 1). Among other things, this paper explores how merger-built S0 galaxies may contribute to the ‘green valley’ population — specifically, involving S0 galaxies *a priori* known to be built through gas-rich major mergers involving S galaxy collisions (Sharples et al. 1983; Bertola et al. 1988a,b; Barnes & Hernquist 1996; Naab & Burkert 2003; Romanowsky & Fall 2012), as opposed to fading S galaxies. Another important distinction that needs

emphasis here is that this concept of dust-rich S0 galaxy formation differs from the idea of S galaxy mergers building (pure) *elliptical* galaxies.

3 DATA

3.1 Galaxy sample and the presence of dust

3.1.1 Galaxies with M_{bh} measurements

Building on Savorgnan & Graham (2016), Davis et al. (2019), and Sahu et al. (2019a), the primary sample is presented in Graham & Sahu (2023a), which tabulates the stellar masses of 104 galaxies and their directly measured black hole masses. This sample covers a range of galaxy morphology, as discussed in Graham (2023c). In general, the E, S, and S0 galaxies were identified as such from a combination of visual inspection and multicomponent decomposition with recourse to kinematic profiles and maps when available. Going beyond Sérsic-bulge + exponential-disc fits (e.g., Andredakis et al. 1995; Seigar & James 1998; Khosroshahi et al. 2000; Graham 2001), the core-Sérsic model was employed when needed, and the disc model could be either truncated, anti-truncated, or inclined rather than always exponential. Furthermore, building on the pioneering work of de Jong (1996) and Prieto et al. (1997), additional components such as bars, which are often more massive than the bulges (Laurikainen et al. 2007), were modelled as a separate component. So, too, were nuclei, ansae, and rings, which can be low in mass yet bias the fitted bulge model due to their significant surface brightness over a small region. Furthermore, radial variations in the isophotal contours, as traced by Fourier Harmonics (Carter 1978; Ohta et al. 1990; Aguerri et al. 2000; Ciambur 2015; Ciambur & Graham 2016) were used to help distinguish (peanut shell)-shaped structures and inner discs, sometimes referred to as pseudobulges, that differ from bulges.

The ES galaxies have intermediate-scale discs rather than the large-scale discs that dominate at large radii in S0 galaxies. Collectively, the above resulted in improved bulge magnitudes that were used in conjunction with the refined morphologies to uncover the morphology-dependent black hole mass scaling relations shown in Fig. 1 and explained in Graham (2023c). This level of sophistication reveals critical departures from the linear $M_{\text{bh}}-M_{*,\text{sph}}$ relation suggested by Dressler & Richstone (1988).

The proximity of the sample means that there is little, albeit some, scope for misclassification of the galaxy morphology. Of particular note is that the S0 galaxies are not treated as a single population but separated according to four ‘dust bins’, encompassing:

- no dust, dust=(N)o,
- not much, only a nuclear dust ring/disc, dust=(n)uclear,
- some weak/wide(r)-spread dust, dust=(y)es, and
- strong dust presence, dust=(Y)es.

Graham (2023b) reports the presence/absence of dust in the S0 galaxies. The literature also reported that those S0 galaxies, which are dust-rich, formed from a major wet merger, while those that are dust-poor did not. Small bulges and undisturbed stellar morphologies are characteristics of these dust-poor S0 disc galaxies.

This sample, with known black hole masses, is used to revisit the colour-(black hole mass) diagram $\text{CM}_{\text{bh}}\text{D}$ in Section 4.3. For the CMD (Sections 4.1 and 4.2), this sample is complemented with LTGs and ETGs from the Virgo Cluster.

¹³ Mass loss from stellar winds may account for up to half the stellar mass.

¹⁴ The term “Green Valley” was an off-the-cuff reference to Arizona’s Green Valley retirement village, implying that the ‘green valley’ in the CMD is where S galaxies go to retire, before becoming ‘red and dead’.

3.1.2 Virgo Cluster LTGs

A sample of 77 (mostly, see below) LTGs in the Virgo Cluster with SFRs greater than $\sim 0.3 M_{\odot} \text{ yr}^{-1}$ is used. The sample is comprised of 74 LTGs from [Graham et al. \(2019\)](#) supplemented with NGC 4407, NGC 4492, and NGC 4496a from [Soria et al. \(2022\)](#), which details the full sample. An array of optical images of the 77 Virgo Cluster LTGs were checked for dust in case ram-pressure stripping had removed it, as is occurring in the (not in sample) S galaxy NGC 4522 ([Kenney & Koopmann 1999](#); [Vollmer et al. 2000](#)). This is perhaps unlikely given the SFRs. Nonetheless, the internal dust corrections are not applicable if the dust has been removed. However, it turns out that the sample is dust-rich, and they also have predominantly low-to-zero bulge-to-total stellar mass ratios (established from $3.6 \mu\text{m}$ images, analysed by the Spitzer Survey of Stellar Structure in Galaxies (S⁴G) ([Sheth et al. 2010](#)) project¹⁵). Some discs, for example, in NGC 4607, appear sufficiently edge-on that it cannot be discerned if a spiral pattern is present. Nonetheless, they are all dust-rich and require a correction to their optical luminosity.

Among the sample, five galaxies stood out. NGC 4429 is an S0 galaxy with a figure-of-eight pattern and (only) a nuclear dust disc, while NGC 4469 is a more dusty counterpart to NGC 4429. NGC 4457 is a dusty S0/S transition galaxy developing a stellar spiral arm, as may be the dust-rich peculiar S0 galaxy NGC 4606, while NGC 4492 represents a slightly earlier phase with dusty spiral arms visible at optical wavelengths but not yet sufficiently developed to show up in the S⁴G $3.6 \mu\text{m}$ image. The above five galaxies are classified here as S0 rather than S galaxies. Corrections for dust in these galaxies are applied. However, stellar masses (Section 3.2) were unavailable for NGC 4429 and NGC 4469 and for one additional S galaxy: NGC 4647. This reduced the working sample to 74, which includes three S0 galaxies. A further three LTGs (NGC: 4303; 4388; and 4501) were removed because they were already in the sample with directly measured black hole masses. Thus, the sample size of additional LTGs is 68, with an additional three S0 galaxies.

3.1.3 Virgo Cluster ETGs

The Virgo Cluster has been a popular target for constructing CMDs (e.g., [Tifft 1969](#); [Visvanathan & Sandage 1977](#); [Sandage & Visvanathan 1978a](#); [Bower et al. 1992](#); [Lisker et al. 2008](#); [di Serego Alighieri et al. 2013](#); [Smith Castelli et al. 2013](#)) Here, a sample of 100 ETGs in the Virgo Cluster with *Hubble Space Telescope* ACS imaging ([Côté et al. 2004](#)) Each S0 galaxy needed to be assigned to one of the four previously mentioned ‘dust bins’ (Section 3.1.1). This task was made easy as the appearance of dust was already noted by [Ferrarese et al. \(2006\)](#). Deviating from [Ferrarese et al. \(2006\)](#), the possible faint dust filament in the low-mass galaxy IC 3468 ($M_{*} \approx 2 \times 10^9 M_{\odot}$) remains elusive and has not been counted. Signs of dust in the rest of the ETG sample were searched for and possibly found in three low-mass galaxies: IC 3025, IC 3492, and VCC 1512, all of which are recognised dIrr/dE transition galaxies with $(g-i)_{\text{AB}} < 0.8$ mag.

A few of the massive ($M_{*} > 10^{11} M_{\odot}$) ETGs have rather weak dust features: NGC 4472 (E/S0, weak lane); NGC 4486 (E, weak filaments); NGC 4406 (S0, weak filaments); and NGC 4382 (S0,pec., weak patches). Although weak filaments may be a sign of minor accretions ([López-Sánchez et al. 2012](#)), the dust patches in

NGC 4382 are regarded in the literature as a fading signature of its merger origin, evident by its stellar shells, ripples, and plume/tail ([Schweizer & Seitzer 1988](#); [Ebneter et al. 1988](#); [Sandage & Bedke 1994](#)). The shells around NGC 4472 ([Spavone 2016](#)) are also indicative of its merger origin, as is its depleted stellar core ([Dullo & Graham 2014](#), and references therein) and bimodal globular cluster system ([Geisler et al. 1996](#)). Once these massive galaxies are immersed in a hot, X-ray-emitting, gas halo ([Benson et al. 2003](#)), the dust is effectively evaporated, returning the metals to the gas phase ([Draine & Salpeter 1979](#); [Khalatyan et al. 2008](#)).

Two low-mass, dust-rich ETGs are also worthy of comment: VCC 1250 (NGC 4476) and VCC 571. The strong ~ 2 kpc dust lane/disc in NGC 4476 ($M_{*} \approx 10^{10} M_{\odot}$) is associated with $10^8 M_{\odot}$ of molecular hydrogen having an external origin ([Tomita et al. 2000](#); [Young 2002](#)). The galaxy is regarded as having experienced a merger event, presumably involving the acquisition of a less massive, gas-rich spiral galaxy, which has led to the different angular momentum of the gas from the bulk of the stars. In general, ETGs with prominent dust lanes tend to be known merger remnants (e.g., [Kaviraj et al. 2012](#); [Yoon & Lim 2020](#)). The other dwarf galaxy, VCC 571 ($M_{*} \approx 10^9 M_{\odot}$), displays a young blue core ([Urich et al. 2017](#); [Hamraz et al. 2019](#)) and is regarded as a transition-type dwarf galaxy by [De Looze et al. \(2013\)](#).

Of the 100 ETGs, nine (NGC: 4374; 4434; 4473; 4486; 4552; 4578; 4621; 4649; and 4762) are already included among the sample with directly measured black hole masses. They are, therefore, removed to give a sample of 91 additional ETGs for use in the CMD. Of these, three are considered here to be dust-rich S0 galaxies (NGC 4476, NGC 4526, and VCC 571).

3.2 Galaxy colours and stellar masses

3.2.1 Galaxies with M_{bh} measurements

The sample with black hole masses had their stellar masses derived by [Graham & Sahu \(2023a\)](#), their equation 4) using *Spitzer Space Telescope* (SST: [Werner et al. 2004](#)) Infrared Array Camera (IRAC: [Fazio et al. 2004](#)) $3.6 \mu\text{m}$ luminosities coupled with the following expression for colour-dependent mass-to-light ratios:

$$\log(M_{*}/L_{3.6}) = 1.034(B - V)_{\text{Vega}} - 1.067, \quad (1)$$

valid for $0.5 < (B - V)_{\text{Vega}} < 1.1$ mag. This equation effectively assumes a diet-Salpeter IMF, as used by [Bell & de Jong \(2001\)](#), and therefore — see [Bell et al. \(2003, p.306\)](#) and [Bernardi et al. \(2010, their table 2\)](#) — it yields logarithmic masses that are 0.15 dex greater than would be obtained assuming a [Kroupa \(2002\)](#) IMF.¹⁶ The $(B - V)_{\text{Vega}}$ colours came from ‘The Third Reference Catalog’ de [Vaucouleurs et al. \(RC3: 1991\)](#), as made available via the *NASA/IPAC Extragalactic Database (NED)*.¹⁷ They were corrected for Galactic extinction using the dust maps from [Schlafly & Finkbeiner \(2011\)](#), also taken from *NED*. Eq. 1 stems from the $(B - V)_{\text{Vega}}$ -dependent expression for the K -band M_{*}/L_K ratios given by [Into & Portinari \(2013, their table 6\)](#). It was based on realistic dusty models, designed for “samples that include a range of morphologies, intrinsic colours and random inclinations”. For blue LTGs with $(B - V)_{\text{Vega}} = 0.7$ mag, Eq. 1 gives $M_{*}/L_{3.6} \approx 0.45$, while

¹⁶ Note: equation 4 from [Graham & Sahu \(2023a\)](#) was mistakenly derived by adding, rather than subtracting, $(0.3 - 0.225) = 0.075$. As such the stellar masses and black hole scaling relations presented there are calibrated to the diet-Salpeter IMF.

¹⁷ <http://nedwww.ipac.caltech.edu>

¹⁵ <https://irsa.ipac.caltech.edu/data/SPITZER/S4G/>

for red ETGs with $(B - V)_{\text{Vega}} = 0.9$ mag, one has $M_*/L_{3.6} \approx 0.73$. The stellar masses obtained from this expression match closely with those obtained using expressions in [Roediger & Courteau \(2015\)](#), [Schombert et al. \(2019\)](#), and [Schombert et al. \(2022\)](#).

3.2.2 Virgo Cluster LTGs

All but three of the Virgo Cluster LTGs had their stellar masses derived using S⁴G 3.6 μm magnitudes¹⁸ coupled with distances from [Soria et al. \(2022, their table 1, column 8\)](#) and use of Eq. 1. [Sahu et al. \(2023\)](#) have shown that the 3.6 μm magnitudes measured by the S⁴G team were derived consistently with the 3.6 μm magnitudes obtained for the sample with directly measured black hole masses ([Savorgnan & Graham 2016](#); [Davis et al. 2019](#); [Sahu et al. 2019a](#)). However, V-band magnitudes were unavailable for 20 of the 68 LTGs in the Virgo Cluster, which meant that $(B - V)_{\text{Vega}}$ colours were unavailable. Of those 20 galaxies, 14 had *Sloan Digital Sky Survey* (*SDSS*: [York et al. 2000](#))¹⁹ $(g - i)_{\text{AB}}$ colours that were corrected for Galactic extinction ([Schlafly & Finkbeiner 2011](#))²⁰ and used to estimate the $(B - V)_{\text{Vega}}$ colour under the approximation seen in Figure 3 and denoted by the relation

$$(g - i)_{\text{AB}} = 1.22(B - V)_{\text{Vega}} + 0.06. \quad (2)$$

To obtain the stellar masses for these 14 Virgo Cluster LTGs, the 3.6 μm luminosities were coupled with

$$\begin{aligned} \log(M_*/L_{3.6}) &= 1.034[(g - i)_{\text{AB}} - 0.06]/1.22 - 1.067 \\ &= 0.848(g - i)_{\text{AB}} - 1.118. \end{aligned} \quad (3)$$

For $(g - i)_{\text{AB}} = 0.9$ mag, one obtains $M_*/L_{3.6} \approx 0.44$. Collectively, Eq. 1 and 3 provided stellar masses for an additional 62 (=68 minus 6 with no $(B - V)_{\text{Vega}}$ nor $(g - i)_{\text{AB}}$ colour) LTGs (plus 3 S0 galaxies) in the Virgo Cluster.

A caveat is that seven of these 62 galaxies have $(g - i)_{\text{AB}}$ colours less than ~ 0.6 mag (see Fig. 4), indicative of a $(B - V)_{\text{Vega}}$ colour less than ~ 0.5 mag (see Fig. 3), thus giving $M_*/L_{3.6} \lesssim 0.3$. The $M_*/L_{3.6}$ ratio may not be reliable for these seven galaxies, such that the actual $M_*/L_{3.6}$ ratio may have been underestimated and more likely be in the range of 0.3–0.4. The models of [Schombert et al. \(2022, their figure 2\)](#) suggest that the ratio may ‘bottom out’ at around 0.36, corresponding to $(g - i)_{\text{AB}} = 0.8$ mag or $(B - V)_{\text{Vega}} = 0.6$ mag. [Into & Portinari \(2013, their figure 10\)](#) reveals this effect with the $M_*/L_{2.2}$ ratio. Given the bluer $(g - i)_{\text{AB}}$ colours of these seven galaxies, this would imply that they may have had their masses underestimated by up to a factor of two, which should be borne in mind when looking at Figs. 4 and 5.

3.2.3 Virgo Cluster ETGs

The bulk of the Virgo Cluster ETGs do not have S⁴G 3.6 μm magnitudes. However, GOLD Mine²¹ ([Gavazzi et al. 2003](#)) 2.2 μm magnitudes are available for all but three of the 91 additional ETGs, and *SDSS ugriz* colours are available for all. This is fortuitous as V-band magnitudes were unavailable for this sample’s fainter half.

¹⁸ Available for all the Virgo Cluster LTGs, excluding NGC 4429, NGC 4469, and NGC 4647, the magnitudes were obtained at <http://cdsarc.unistra.fr/viz-bin/nph-Cat/html?J/PASP/122/1397/s4g.dat.gz>

¹⁹ <https://www.sdss3.org/>

²⁰ The $(g - i)_{\text{AB}}$ colours and Galactic extinctions were taken from *NED*.

²¹ <http://goldmine.mib.infn.it/>

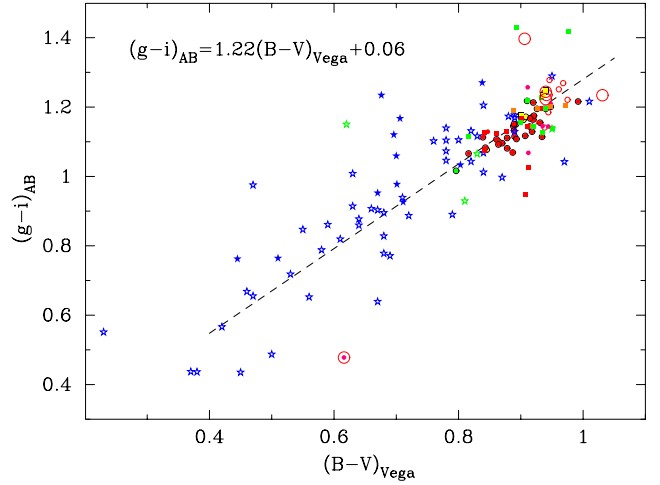


Figure 3. (Galactic extinction)-corrected *SDSS* $(g - i)_{\text{AB}}$ colour versus (Galactic extinction)-corrected *RC3* $(B_T - V_T)_{\text{Vega}}$ colour. (The subscript T denotes total galaxy magnitudes, but is dropped elsewhere for convenience.) The dashed line is a simple approximation of the distribution. The elliptical (ES) BCG with $(g - i)_{\text{AB,obs}} = 0.48$ mag is NGC 1275, affected by an AGN. Symbols have the same meaning as in Fig. 1. Also shown are additional Virgo Cluster LTGs (open blue stars) plus three misclassified Virgo Cluster S0 galaxies (open green stars, see Section 3.1), along with additional Virgo Cluster ETGs denoted by the new circles that are colour-coded according to the galaxy ‘dust bins’: Y (green); y (yellow); n (orange); and N (red). See Section 3 for details.

Therefore, the $(g - i)_{\text{AB}}$ colour — which tracks the $(B - V)_{\text{Vega}}$ colour (Fig. 3, Eq. 2) — has been used.

[Graham & Sahu \(2023a\)](#) note that the equation

$$\log(M_*/L_K) = 1.055(B - V)_{\text{Vega}} - 1.066 (+0.075) \quad (4)$$

from [Into & Portinari \(2013, their table 3\)](#)²² — from a simpler galaxy model — might be more applicable for ETGs. [Graham & Sahu \(2023a, see their figure 1\)](#) also reveal that it matches well with the $(B - V)_{\text{Vega}}$ -dependent expression for M_*/L_K ratios given by [Into & Portinari \(2013, their table 6\)](#) for the dusty galaxy model that was used to derive Eq. 1. For $(B - V)_{\text{Vega}} = 0.7$ mag, Eq. 4 gives $M_*/L_{2.2} \approx 0.56$; for $(B - V)_{\text{Vega}} = 0.9$ mag, one obtains $M_*/L_{2.2} \approx 0.91$. Eq. 2 can be used to modify Eq. 4, such that

$$\log(M_*/L_{2.2}) = 0.865(g - i)_{\text{AB}} - 1.043. \quad (5)$$

For $(g - i)_{\text{AB}} = 0.91$ mag, one obtains $M_*/L_{2.2} \approx 0.55$; for $(g - i)_{\text{AB}} = 1.16$ mag, one obtains $M_*/L_{2.2} \approx 0.91$.

Section 4.1 presents the galaxies’ (Galactic extinction)-corrected $(g - i)_{\text{AB}}$ colours plotted against their stellar masses. In Section 4.2, these colours are additionally corrected for dimming due to dust in the galaxies. The above expressions for M/L are purportedly applicable to dusty models and a range of galaxy morphologies and colours. The revised colours are not used to adjust the stellar masses, although this could be explored in future work.

3.3 Correcting for dust

Using galaxy samples with different disc inclinations, [Driver et al. \(2007a\)](#) utilised the turnover luminosity, L^* , of each sample’s

²² The modification here is the adjustment by 0.075 dex to switch from a [Kroupa \(1998\)](#) IMF to a [diet-Salpeter IMF \(Bell et al. 2003\)](#).

(bulge and disc) luminosity function to track the average extinction as a function of disc inclination. Their work also included an adjustment for dimming due to dust in face-on discs. These sample-averaged corrections are applied to individual galaxies based on their disc inclination. Individual galaxies may, of course, have less or more dust than the average disc galaxy. Thus, these inclination-dependent dust corrections can be too large or too small, respectively, when applied individually. However, when dealing with an ensemble of N galaxies, as done here, this average dust correction works because the error in the mean shift to the cloud of points declines with \sqrt{N} . Driver et al. (2008) expanded the application to include the use of the *SDSS ugriz* filter set, and the corrections given there are applied here to the S galaxies and the S0 galaxies with dust=Y (Graham 2023b), including two ES,b galaxies.²³

The dust corrections to a galaxy's bulge and disc magnitude, \mathfrak{M} , can be combined to give the intrinsic galaxy magnitude from the observed magnitude²⁴, such that

$$\mathfrak{M}_{\text{gal,intrin}} = \mathfrak{M}_{\text{gal,obs}} - 2.5 \log \left\{ \left(\frac{B}{T} \right)_{\text{obs}} 10^{\Delta \mathfrak{M}_{\text{bulge}}/2.5} + \left[1 - \left(\frac{B}{T} \right)_{\text{obs}} \right] 10^{\Delta \mathfrak{M}_{\text{disc}}/2.5} \right\} \quad (6)$$

where $(B/T)_{\text{obs}}$ is the observed bulge-to-total luminosity ratio, and non-bulge components such as bars and rings are effectively considered a part of the disc. The corrective terms are such that

$$\Delta \mathfrak{M}_{\text{bulge}} = \mathfrak{M}_{\text{bulge,obs}} - \mathfrak{M}_{\text{bulge,intrin}} = b_1 + b_2 [1 - \cos(i)]^{b_3}, \quad (7)$$

and

$$\Delta \mathfrak{M}_{\text{disc}} = \mathfrak{M}_{\text{disc,obs}} - \mathfrak{M}_{\text{disc,intrin}} = d_1 + d_2 [1 - \cos(i)]^{d_3}, \quad (8)$$

where the coefficients b_1 to b_3 and d_1 to d_3 are passband-dependent and given in Driver et al. (2008). The (cosine of the) disc inclination angle, i , is such that $i = 90$ degrees for an edge-on disc and $i = 0$ degrees for a face-on disc. This correction to the observed galaxy luminosity therefore requires the disc inclination and the B/T flux ratio.

For the galaxy sample with directly measured values of M_{bh} , their $(B/T)_{3.6}$ ratios are available from (Graham & Sahu 2023a). For that sample's LTGs, their disc inclinations are provided by Davis et al. (2017), and for the dust-rich S0 galaxies, $\cos i$ is roughly equal to the observed (projected on the plane-of-the-sky) minor-to-major axis ratio, b/a , at the radii where the disc dominates. More specifically, an average ratio of vertical scale height, z , to radial scale length, h , i.e., disc thickness, of 0.25 (e.g., Sandage et al. 1970; Bizyaev et al. 2014, their figure 4) is assumed. This ratio is also adopted for the three additional dust-rich S0 galaxies in the Virgo cluster without a direct M_{bh} measurement, while a thickness of 0.21 (Padilla & Strauss 2008) is adopted for the Virgo Cluster's LTGs without M_{bh} measurements. These z/h ratios are used in the equation

$$\cos^2(90 - i) = \frac{1 - (b/a)^2}{1 - (z/h)^2} \quad (9)$$

from Hubble (1926) to establish the inclinations of the discs not listed by Davis et al. (2017). For the Virgo Cluster LTGs without a directly measured black hole mass, their observed b/a axis ratios came from Sheth et al. (2010), and their $3.6 \mu\text{m}$ B/T ratios were

reported by Salo et al. (2015).²⁵ For the Virgo Cluster ETGs without a directly measured black hole mass, there are just three dust-rich galaxies requiring a dust correction. NGC 4526 ($b/a = 0.33$), which resembles NGC 2787, has been assigned $(B/T)_{2.2} = 0.2$, while the lower-mass galaxies NGC 4476 ($b/a = 0.68$) and VCC 571 ($b/a = 0.52$) have been assigned $(B/T)_{2.2} = 0.1$.

At $3.6 \mu\text{m}$, Eq. 6 is not required. Indeed, rather than obscuring the starlight, star-heated warm dust glows at $3.6 \mu\text{m}$. In LTGs, this typically accounts for ~ 25 per cent of the $3.6 \mu\text{m}$ luminosity (Meidt et al. 2014). At $2.2 \mu\text{m}$, the corrective term in Eq. 6 is typically ~ 0.1 mag, and it is ignored here for the three dust-rich S0 galaxies from the Virgo Cluster ETG sample for which Gold MINE $2.2 \mu\text{m}$ luminosities were used. Due to the higher concentration of dust in the centres of galaxies and the blue colours of star-forming discs, the B/T flux ratio decreases when we observe dusty disc galaxies at bluer wavelengths, as seen in, for example, Graham (2001, figure 15), Möllenhoff (2004, figures 5-6), Graham & Worley (2008, figure 7), and more generally Vika et al. (2014), Kennedy et al. (2016), and Häußler et al. (2022). In the absence of multicomponent decompositions in the *SDSS ugriz* bands for the current data samples, the $(B/T)_{3.6}$ (and $(B/T)_{2.2}$ for three S0 galaxies) ratios were simply reduced by a factor of 1.0, 1.0, 0.5 and 0.25 to give the corresponding ratios in the z , i , g , and u bands, respectively (see Section A and Möllenhoff (2004, figures 6) for the u -band). These ratios are used in Eq. 6 to correct the *ugiz* galaxy magnitudes for dust.

Among the sample with directly measured black hole masses, there are five dust-rich elliptical-like galaxies for which the dust corrections (designed for galaxies with large-scale discs) are problematic. These are comprised of one dust-rich elliptical galaxy (NGC 4374), two dust-rich elliptical ES,e type galaxies (NGC 1275 and NGC 3607), and the two dust-rich elliptical ES,b type galaxies (NGC 3115 and NGC 6861). While NGC 4374 has a negligible SFR, NGC 3607 has been measured to form stars at a rate of $0.25 M_{\odot} \text{ yr}^{-1}$ (Graham et al. 2023), and arguably may require a dust correction. NGC 1275 is very blue due to its AGN (Irwin et al. 2001) and should be disregarded. In the past, ES,e and ES,b galaxies would tend to be misclassified as (ordinary) E and (compact) S0 galaxies, respectively. Here, the dust correction is applied to just the two ES,b galaxies, but this has little impact on the overall trends displayed by the larger sample.

4 ANALYSIS AND INTERPRETATION

4.1 The observed CMD

The $(g - i)_{\text{AB}}$ colour versus stellar mass diagram (Fig. 4, left-hand side) resembles the $(B - V)_{\text{vega}}$ colour versus $3.6 \mu\text{m}$ absolute magnitude diagram for the sample with directly measured black hole masses (Graham & Sahu 2023a, their figure 1). This is indicative of the $(g - i)_{\text{AB}}$ colour broadly tracing the $(B - V)_{\text{vega}}$ colour and the relatively narrow range of $M/L_{3.6}$ ratios. In the right-hand side of Fig. 4, the CMD extends to lower-mass galaxies due to including the Virgo Cluster galaxies. Reassuringly, the general pattern seen on the right-hand side of Fig. 4 for the ETGs from the Virgo Cluster matches the $g' - i'$ CMD shown by Roediger et al. (2017, their figure 2). The general trend also matches that seen elsewhere, such as

²³ As noted in Section 2.1, ES,b galaxies seem more akin to S0 galaxies than E galaxies.

²⁴ In practice, $\mathfrak{M}_{\text{gal,obs}}$ was first corrected for dust in our galaxy using the extinction maps of Schlafly & Finkbeiner (2011).

²⁵ <https://irsa.ipac.caltech.edu/data/SPITZER/S4G/overview.html>, see also https://www.oulu.fi/astronomy/S4G_PIPELINE4/MAIN/

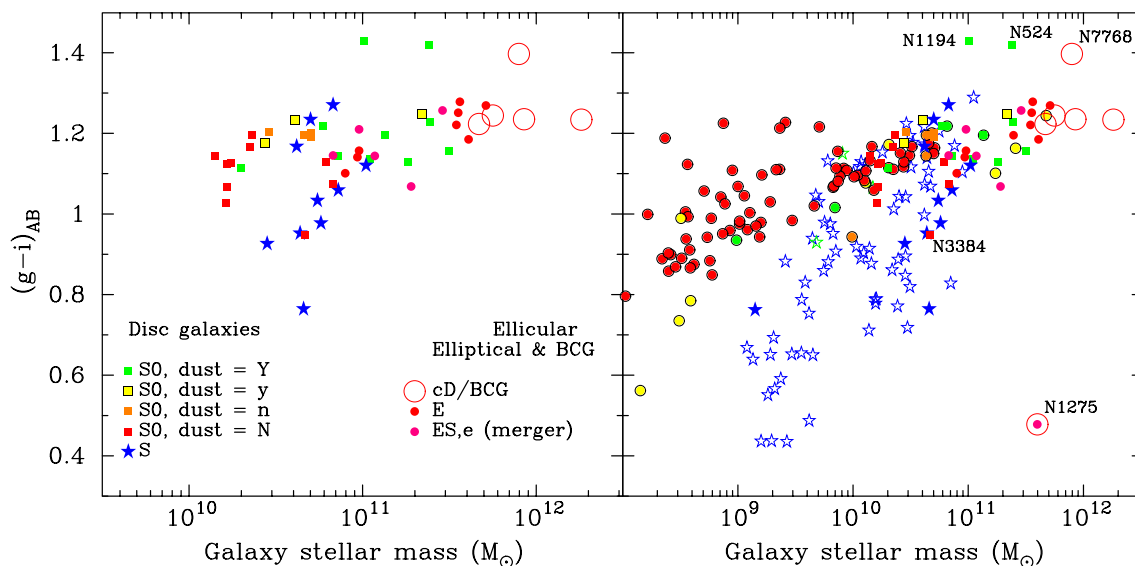


Figure 4. Left panel: Colour-mass diagram for the sample having both directly measured black hole masses and *SDSS* colours (including the dusty galaxy NGC 1275 with an AGN). Corrections for Galactic dust extinction have been made, but not for dust in the external galaxies. Right panel: Addition of 62 Virgo Cluster LTGs (open blue stars) plus three misclassified Virgo Cluster S0 galaxies (open green stars, see Section 3.1) and 88 (= 100 – 9 – 3) Virgo Cluster ETGs denoted by the new circles that are colour-coded according to the galaxy ‘dust bins’: Y (green); y (yellow); n (orange); and N (red). See Section 3 for details.

reported by [Boselli & Gavazzi \(2014\)](#) and [Schombert \(2018\)](#). Thus far, only a correction for dust in our Galaxy ([Schlafly & Finkbeiner 2011](#)), courtesy of *NED*, has been applied to the optical colours in Fig. 4. Therefore, one aspect which can be improved is to apply a correction for dust in the external galaxies.

4.2 The intrinsic CMD: Dust corrections in external galaxies

Fig. 5 reveals the shift in the CMD after correcting for dust. It illustrates that dust-corrected S0 galaxies, which contribute to the ‘green mountain’, are co-located with S galaxies at the high-mass green end of the ‘blue cloud’ ([Bravo et al. 2022](#)). These dust-rich S0 galaxies could be the population bolstering the ‘green valley’ seen by [Martin et al. \(2007\)](#); [Wyder et al. \(2007, their figure 11\)](#) in the *GALEX* near-ultraviolet (NUV)-(*SDSS*) optical CMD.

During wet (gas-rich) mergers of S galaxies, the gas particles, unlike the stars — which are separated by vast distances —, have high number densities, leading them to interact with each other. As a result, some gas particles lose speed and fall inward, while others get heated to high temperatures. The merging of these galaxies leads to the creation of central gas systems, which may be associated with considerable AGN activity initially ([Tomita et al. 2000](#)). It is speculated here that this may also be the origin of some (tens to hundreds of pc sized) nuclear discs in massive ETGs (e.g., [Rest et al. 2001](#)); in contrast to the smaller, more spheroidal, nuclear star clusters found in low-mass ETGs and LTGs (e.g., [Böker et al. 2002](#); [Balcels et al. 2007](#); [Scott & Graham 2013](#)).

[Bait et al. \(2017, their figure 10\)](#) suggest that the starbursting S0 galaxies evolve rapidly from the ‘blue cloud’ to the ‘green valley’. [Brammer et al. \(2009, see their figure 4\)](#) note that dusty starbursts can appear in the ‘green valley’ on the ‘red sequence’ but that many shift back into the ‘blue cloud’ after correcting for dust. [Schawinski et al. \(2014\)](#) also observed a probable S/S0 cohabitation/dual occupancy in the CMD, where the bulk of their ‘green valley’ sample of unknown “indeterminate” galaxy type overlap with the high-mass green end of the S galaxies’ ‘blue

cloud’. However, while [Schawinski et al. \(2014\)](#) speculated that these overlapping unknown galaxy types were faded S galaxies, some/many may instead be merger products. It is important to note that three of the four best candidates for faded S galaxies in the current sample reside on the ‘red sequence’ rather than still tapering off from the ‘blue cloud’. This favours rapid cold gas removal mechanisms acting on some S galaxies, at least in the present sample, to move them quickly through the ‘green valley’ (e.g., [Barway et al. 2009](#); [Kelvin et al. 2018](#)), rather than gradual consumption of their cold gas via declining star formation effectively leaving them as S galaxies in the green end of the ‘blue cloud’ [Schawinski et al. \(2014\)](#).

In Fig. 6, the large arrows denote the galaxy-merger-induced transformations. For those disc galaxies that did not develop a spiral pattern, perhaps due to an early entry into a proto-cluster environment with a hot gas halo, they would have become today’s ($z = 0$) dust-poor S0 galaxies. If gas acquisitions, gas recycling (e.g., [Ciotti et al. 1991](#)), and minor mergers are sufficient to keep a disc fuelled and cause gravitational perturbations that produce/maintain a spiral pattern, then an S galaxy arises ([Lin & Shu 1964](#); [Julian & Toomre 1966](#); [D’Onghia et al. 2013](#)). However, the S0 → S passage is likely the domain of a bygone era when the Universe was fuelling galaxies at a greater rate. Today ($z = 0$), gas accretion onto a dust-poor S0 galaxy might only be sufficient to move it into the ‘green valley’ due to limited star formation (e.g., [Hau et al. 2008](#); [Kannappan et al. 2009](#); [Mapelli 2015](#)), in part because of inclined, off-plane accretion ([Sil’chenko et al. 2019](#)) and the high angular momentum of the accreted gas ([Peng & Renzini 2020](#)). This subdued level of star formation is known as ‘rejuvenation’ ([Goudfrooij et al. 1990](#); [Schweizer & Seitzer 1992](#); [Tantalo et al. 1998](#); [Rampazzo et al. 2007](#); [Thilker et al. 2010](#); [Mapelli 2015](#); [Rathore et al. 2022](#)). At $z = 0$, this is expected to be more common in the lower mass galaxies where the accreted material has a greater chance of being a higher fraction of the galaxy’s mass. This can be thought of as a kind of ‘downsizing’. A reverse (S → dust-poor S0) process involves the rapid (stripping) or slow (consumption and exhaustion)

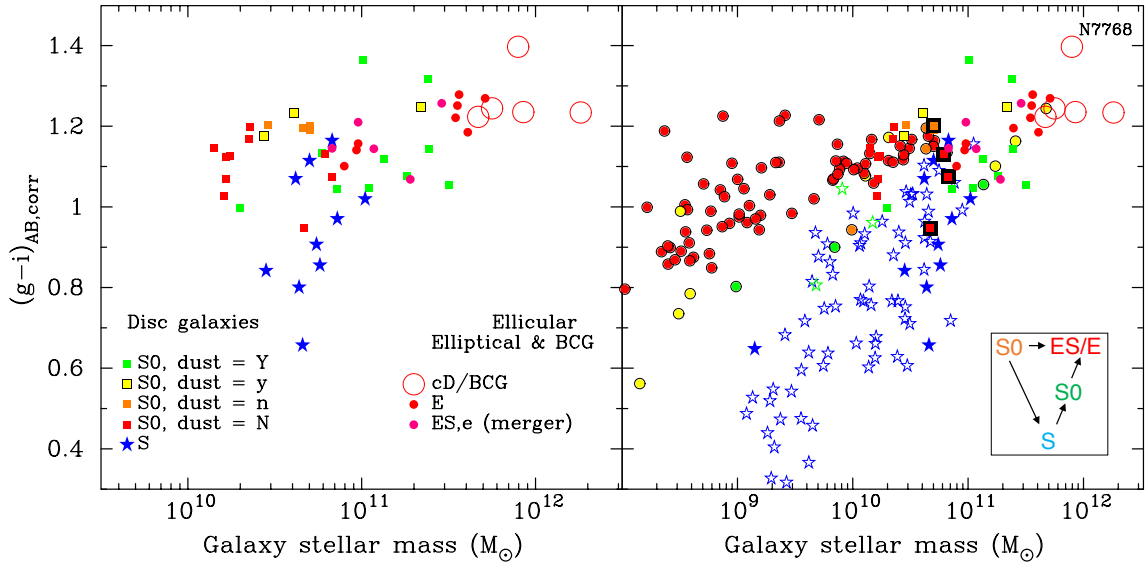


Figure 5. Similar to Fig. 4, except that the $(g-i)_{AB}$ colour has additionally been corrected for dust in the external galaxies using the (disc inclination)-dependent prescription described in Section 4.2 and following Driver et al. (2008). The AGN NGC 1275 has been removed. Four dust-poor S0 galaxies that are possibly faded and transformed S galaxies are enclosed in a thick black square, contributing to the three types of S0 galaxy: primordial, wet-merger built, and faded S. Spiral patterns emerge, often long ago, in what were initially spiral-less discs, and collisional weddings, i.e., major mergers, also drive galaxy speciation, captured by the ‘Triangular’ (Graham 2023c).

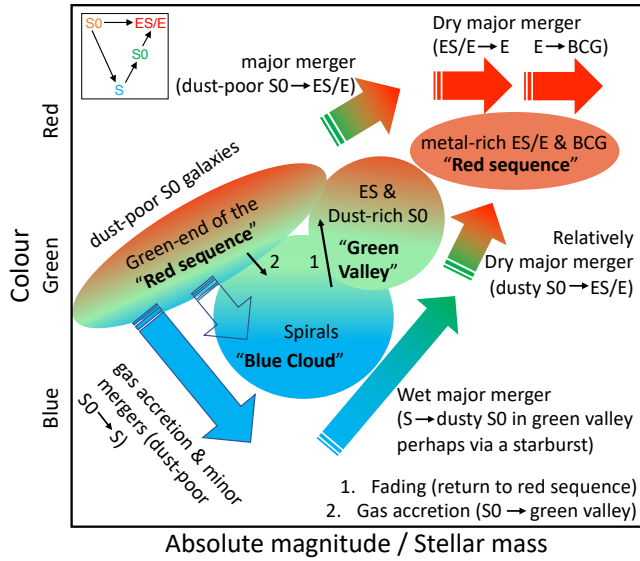


Figure 6. Cartoon colour-mass diagram. The large arrows show major evolutionary paths (punctuated equilibrium) taken by galaxies. The triangular-like structure introduced by Graham (2023c) and seen in Fig. 2 is evident. Most S0-to-S transitions likely occurred in the past, when spiral patterns were induced in pre-existing discs, while the S-to-S0 merger-induced transitions are expected to occur in the past, present, and future. Most distant-future mergers are expected to be dry mergers. Today ($z = 0$), incomplete S0-to-S transitions may yield dwarf ETGs with blue cores. Tidal stripping may produce overly red dwarf galaxies for their (reduced) stellar mass, including compact E (cE) galaxies and tidal thrashing may produce ultracompact dwarf (UCD) galaxies. Some ES galaxies are closely associated with dust-rich S0 galaxies in the diagram; that is, there is some overlap rather than sharp dichotomies.

removal of fuel, which can snuff out star formation and return a blue galaxy to the ‘red sequence.’

Major merging of gas-rich S galaxies can result in a burst of star formation and transform a pair of S galaxies into a dust-rich S0 galaxy along the ‘green range’. Rather than a ‘valley’ or deficit between the ‘blue cloud’ and ‘red sequence’, there (i) may be something of a ‘mountain’ or excess at $M_* \sim 10^{11} M_\odot$ and (ii) an additional population ranging to lower masses. Although more data would be desirable, the dust-rich S0 galaxies appear to form a mid-to-low mass ridge on the green side of the ‘red sequence’ (Fig. 4) and ‘blue cloud’ (Fig. 5). The higher abundance of merger-built dust-rich S0 galaxies at higher masses may reflect a greater propensity for wet mergers to occur due to the stronger gravitational attraction of more massive systems that are better able to turn (otherwise flyby) encounters at a given velocity into mergers.

4.3 The colour-(black hole mass) diagram: $CM_{bh}D$

Given that galaxy masses are not required for the $CM_{bh}D$, expanding the sample of galaxies with directly measured black hole masses is possible. Of the 145 galaxies with directly measured black hole masses listed in Sahu et al. (2019b), 70 have both g and i *SDSS* magnitudes in the *NED* database, and 69 have both *SDSS* u and z magnitudes. There are 59 having both *SDSS* u and *Spitzer* [3.6] magnitudes. These latter magnitudes encompass three galaxies with S^4G -derived [3.6] galaxy magnitudes, with the remainder coming from Savorgnan & Graham (2016), Davis et al. (2019), Sahu et al. (2019a), and Graham & Sahu (2023b). Fig. 7 shows M_{bh} against the *SDSS* $(g-i)_{AB}$ and $(u-z)_{AB}$ colours and the *SDSS*-*Spitzer* $(u-[3.6])_{AB}$ colour. These colours are yet to be corrected for dust in the external galaxies; they have only been corrected for dust in our galaxy.

After Savorgnan et al. (2016) suggested there was a red and blue sequence in the $M_{bh}-M_{*,sph}$ diagram — which has been supplanted by the (galaxy morphology)-dependent relations seen in

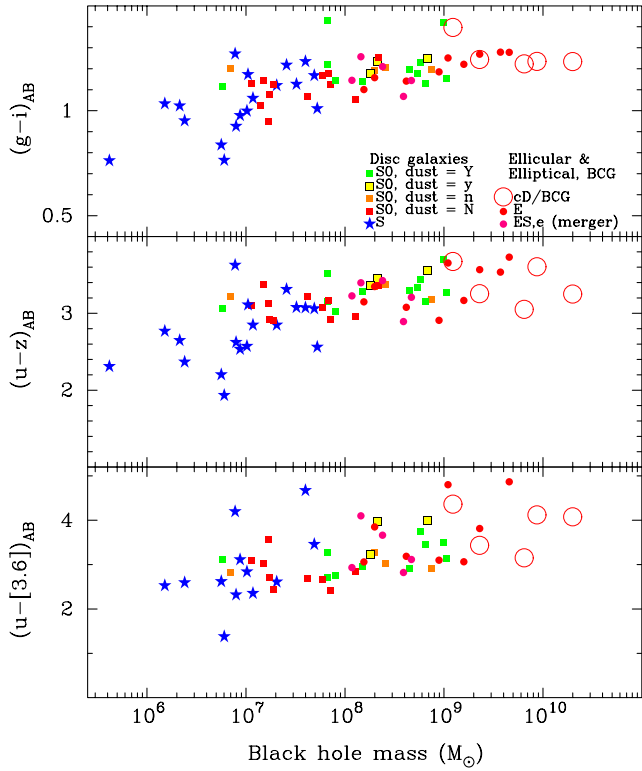


Figure 7. Colour-(black hole mass) diagram (CM_{bhD}) for galaxies with directly measured black hole masses and available *SDSS* colours. Top panel: The reported separation between ETGs and LTGs seen in the $M_{bh}-M_{*,galaxy}$ diagram by [Dullo et al. \(2020\)](#) is not (yet) evident here. The distribution appears to asymptote in the red. The three galaxies with $(g-i)_{AB} \approx 1.4$ mag may be measurement errors. While the Galactic extinction correction is applied here, no correction for dust internal to the galaxies has been applied.

Fig. 1 — [Dullo et al. \(2020\)](#) introduced red and blue M_{bh} -colour relations. That study coupled *Galaxy Evolution Explorer* (*GALEX*; [Morrissey et al. 2007](#)) ultraviolet and *Spitzer* infrared magnitudes for 67 galaxies to provide FUV-[3.6] and NUV-[3.6] colours. [Dullo et al. \(2020\)](#) reported separate blue and ‘red sequences’ for LTGs and ETGs (E, S0, and S0/a). This division is not (yet) apparent in the current sample (Fig. 7). This is, in part, likely due to the low number of S galaxies, in particular at $10^7 < M_{bh}/M_{\odot} < 10^8$. It is also, as shown next, partly because of the dust in the external galaxies.

[Dullo et al. \(2020\)](#) used the dust corrections from [Driver et al. \(2008\)](#) to present the M_{bh} -colour diagram, using *GALEX* and *Spitzer* magnitudes for the colour. Given that [Driver et al. \(2008\)](#) only provided corrections from u to K [$2.2 \mu\text{m}$], [Dullo et al. \(2020\)](#) adapted the correction in the u -band for their *GALEX* UV data, and the correction in the K -band for their *Spitzer* $3.6 \mu\text{m}$ data. The approach taken here differs slightly in a few other ways. First, while [Dullo et al. \(2020\)](#) used the same corrective formula as [Driver et al. \(2008\)](#), they only applied it to the LTGs and not to the dust-rich S0 galaxies. This makes the LTGs’ colours more blue relative to all the ETGs, enhancing the separation in colour. A second (minor) difference is that [Dullo et al. \(2020\)](#) used $\cos i = b/a$ to establish the inclination of the discs; that is, they assumed the discs were infinitely thin (cf., Eq. 9). Third, they applied the dust-dimming correction to brighten the $3.6 \mu\text{m}$ magnitudes of the LTGs. For a

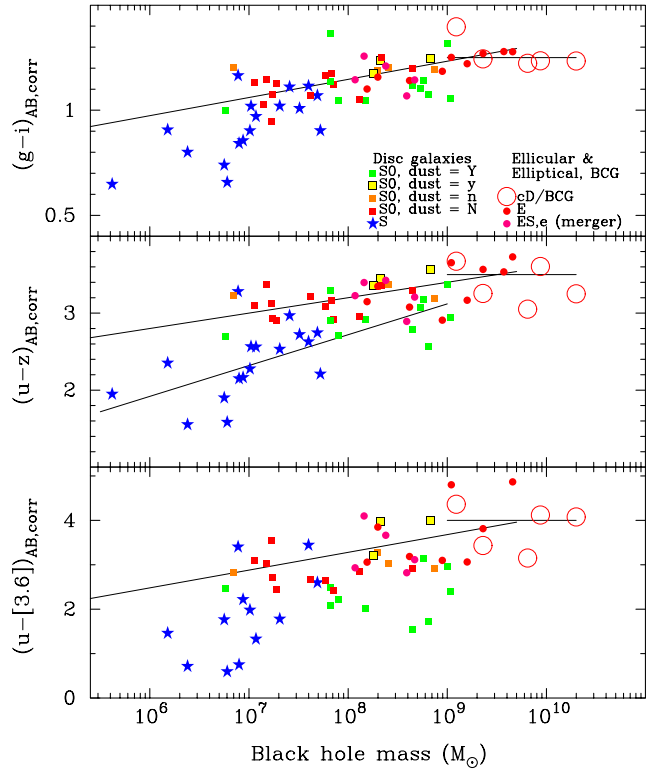


Figure 8. Similar to Fig. 7 but with (disc inclination)-dependent dust-corrections applied to the S and dust-rich (dust=Y) S0 galaxies. The two red spirals with $(u-[3.6])_{AB,corr} > 3$ mag are NGC 3368 and NGC 4258. Parallels with the CMD (Fig. 5 and 6) are evident, helping to explain the CM_{bhD} shown here, where one can detect a ‘red sequence’ with a ‘red plateau’ and a blue-green sequence/cloud with a green mountain/range. Relations for the S and dust-rich S0 galaxies and for the dust-poor S0 and ES/E/BCG galaxies are given by Eq. 13 and 10–12, respectively.

disc-dominated LTG with a projected (on the plane of the sky) axis ratio $b/a = 0.25$, this amounts to a brightening of ~ 0.18 mag. However, dust does not cause dimming at $3.6 \mu\text{m}$ but instead glows.

Fig. 8 builds on the blue (star-forming) sequence and red (quiesced) sequence shown in [Dullo et al. \(2020\)](#). Although it would be desirable to have a greater number of S galaxies at $10^7 < M_{bh}/M_{\odot} < 10^8$ and more dust-poor S0 galaxies at $M_{bh} < 10^7 M_{\odot}$, as seen in Fig. 5, the ETG/LTG separation seen by [Dullo et al. \(2020\)](#) when using the UV-[3.6] colour is evident in Fig. 8. As suggested for the $M_{bh}-M_{*,gal}$ diagram (Fig. 1, right-hand side), the S and dust-rich S0 galaxies appear to form a sequence when partnered. The blue sequence in [Dullo et al. \(2020\)](#) is modified here to give a blue-green sequence that now includes S and dust-rich S0 galaxies, invariably recognised in the literature as built from wet major mergers likely involving one or two S galaxies ([Graham 2023b](#), see the references therein). Many of these dust-rich S0 galaxies still have residual star formation ([Graham et al. 2023](#)). The red ‘sequence’ is also modified here by excluding the dust-rich S0 galaxies and recognising the near-constant colour for the (pure) E galaxies, creating a plateau at the high-mass end.

The $M_{bh}-(g-i)$ relation shown in the upper panel of Fig. 8 for the ‘red sequence’ (now excluding the dust-rich S0 galaxies) is given by

$$\log M_{bh} = 11.6[(g-i)_{AB,corr} - 1.0] + 6.3, \quad (10)$$

with a red plateau at $(g - i)_{\text{AB,corr}} = 1.25$ mag for $M_{\text{bh}} \gtrsim 10^9 M_{\odot}$. The corresponding $M_{\text{bh}}-(u - z)$ relation shown in the middle panel is such that

$$\log M_{\text{bh}} = 5[(u - z)_{\text{AB,corr}} - 3.0] + 7.0, \quad (11)$$

with a red plateau at $(u - z)_{\text{AB,corr}} = 3.5$ mag. Finally, the ‘red sequence’ in the lower panel is given by

$$\log M_{\text{bh}} = 2.5[(u - [3.6])_{\text{AB,corr}} - 3.0] + 7.3, \quad (12)$$

with a red plateau at $(u - [3.6])_{\text{AB,corr}} = 4.0$ mag.

The tentative relation for the blue-green sequence of LTGs and dust-rich S0 galaxies is less secure due to the dependence of these galaxy colours on the dust-inclination correction. The following expression is shown in the middle panel of Fig. 8:

$$\log M_{\text{bh}} = 2.5[(u - z)_{\text{AB,corr}} - 3] + 8.7. \quad (13)$$

Use of this blue-green relation to predict M_{bh} requires correcting the u and z magnitudes of one’s disc galaxy (sample) for dust and disc inclination. The M_{bh} versus FUV- and NUV-[3.6] colour relations for LTGs in [Dullo et al. \(2020\)](#) also require correcting for dust and disc inclination, and knowledge of the B/D flux ratio after excluding the flux of bars, which can be substantial.

Admittedly, the colour does not appear exceptionally useful for predicting M_{bh} , with a $\pm 2\sigma$ scatter of around ± 1 dex for the red and blue sequences. However, this is competitive with recent $M_{\text{bh}}-\sigma$ relations ([Saglia et al. 2016](#); [Sahu et al. 2019b](#)). This is, however, an evolving area of research, and future refinements to colours, from improved dust corrections, could alter the landscape. The main thrust of this subsection was to understand better the origin of the M_{bh} -colour relations, rather than precisely define the relations, and to see if and how the ‘Triangal’ plays out in the CM_{bhD} .

5 DISCUSSION

This section discusses the rationale for and understanding of the evolutionary pathways in the CMD. Simulations predict disc galaxies condensed from the gravitational collapse of high angular momentum gas clouds ([Frenk et al. 1985](#); [Kauffmann et al. 1993](#); [Stringer & Benson 2007](#); [Zavala et al. 2008](#)), and many redshift-zero low-mass ETGs are disc-dominated galaxies (e.g., [Fall & Efstathiou 1980](#)). They need not have ever hosted a spiral pattern. As such, a high specific angular momentum in galaxies today need not be evidence of a faded spiral galaxy ([Rizzo et al. 2018](#)). Models for spiral formation commence with a perturbation in a pre-existing disc, and spiral patterns undoubtedly flourished in many of the initially spiral-less discs, with ceers-2112 an example distant spiral at $z \approx 3$ ([Costantin et al. 2023](#)); see also A1689B11 at $z = 2.54$ ([Yuan et al. 2017](#)) and possibly BRI 1335-0417 at $z = 4.41$ ([Tsukui & Iguchi 2021](#)).

The $z = 0$ stellar masses of dust-poor S0 galaxies reach up to a few $10^{10} M_{\odot}$. Substantial mergers and accretions appear to have been inevitable above this threshold, resulting in an evolution of their galaxy type (Fig. 1). These low-mass ETGs can have younger (luminosity-weighted) stellar populations than high-mass ETGs (e.g., [Caldwell et al. 2003](#), their figure 21). As such, they are not blue/green relative to high-mass ETGs solely because of a lower metallicity ([Conselice et al. 2003a](#)). However, it must be noted that most (>90 per cent by mass) of the stellar population in low-mass ETGs is thought to be old ([Lisker et al. 2006](#)). Many are essentially a primordial galaxy population, i.e., a first incarnation/generation,

and they can possess a low bulge-to-total ratio ([Graham 2023c](#), figure A2).²⁶ This is also the case with the bulk (>75 per cent) of the stellar mass in the bulges of S galaxies ([MacArthur et al. 2009](#)), with star formation predominantly occurring in the disc where gas clouds cool and condense. By and large, these low-mass dust-poor S0 galaxies in the nearby Universe are metal-poor and may allow us to learn about the early Universe and test our theories of early disc galaxy formation and growth (e.g., [Navarro & White 1994](#); [Khalatyan et al. 2008](#); [Kazantzidis et al. 2011](#); [Pawlik et al. 2011](#); [Prieto et al. 2013](#)). Their mere existence today suggests that the galaxies at cosmic dawn could have been spiral-less disc galaxies, and their $M_{\text{bh}}/M_{*,\text{sph}}$ ratios imply they are not faded S galaxies.

Disc galaxies with a sustained fuel supply may have grown into S galaxies. Minor mergers can build bulges by bringing in material and transplanting disc stars, halo gas can cool, and these mechanisms, along with star-forming turbulence, can produce gravitational perturbations that invoke spiral formation ([Julian & Toomre 1966](#); [Bertin & Lin 1996](#)). The subsequent major merger of S galaxies can destroy the spirals, transfer some disc and bar stars to the bulge component through violent relaxation, but not fully erase the angular momentum ([Barnes & Hernquist 1996](#)), creating the dust-rich S0 galaxies that tend to have more massive bulges and black holes than the S galaxies (Fig. 1, left-hand side). The existence of these more massive bulges in ‘green valley’ galaxies was noted by [Bremer et al. \(2018\)](#). Once they no longer look like mergers-in-progress, and the recent/current star formation has sufficiently declined for the colour to change from blue to green, detecting signs of mergers and interactions in galaxies beyond the local ($z \lesssim 0.03$) Universe becomes quite challenging. This may hamper some studies’ ability to detect the role of mergers in populating the ‘green valley’.

The lynchpin of the Tuning Fork diagram, connecting S and E galaxies, is the (once thought to be singular in origin) S0 galaxy ([Reynolds 1925](#); [Hubble 1936](#)). Astronomers used the S0 galaxy to try and discern how/if galaxies may change from one type to another. [Spitzer & Baade \(1951\)](#) envisaged that high-speed collision between two spiral galaxies in a cluster may lead to the passage of the stars past each other while the much higher number density of the gas particles results in them colliding and being left behind. They suggested this as a means to produce gas-poor S0 galaxies. This scenario was preferred before hot X-ray gas halos in clusters were known. [Gunn & Gott \(1972\)](#) and [Davies & Lewis \(1973\)](#) subsequently advocated for the more efficient process in which the pervasive hot gas ‘ram-pressure’ strips the cool star-forming gas from S galaxies, and the mechanism proposed by [Spitzer & Baade \(1951\)](#) declined in popularity as the idea of altering single S galaxies, rather than pairs, rose in popularity. It was also speculated that S galaxies may collide to produce E-like galaxies (e.g., [Baade & Minkowski 1954](#); [Baldwin & Elsmore 1954](#); [Minkowski & Aller 1954](#)). In group and field environments, where galaxy approach speeds are sufficiently slow, a collision will result in the bulk of the ‘over-shooting’ stars falling back in, resulting in a merger product that is gas- and dust-rich (e.g., [Mazzarella et al. 1991](#); [Whitmore & Schweizer 1995](#)).

Following these two popular mechanisms proposed for cre-

²⁶ S0 galaxies with low bulge-to-total stellar mass ratios are absent from the schematic in [Graham et al. \(2016, their figure 7\)](#) because it implicitly focussed on ‘ordinary’/non-dwarf galaxies with $M_{*,\text{gal}} \gtrsim 10^{10} M_{\odot}$. This encompasses the dust-rich S0 galaxies that typically have higher B/T stellar mass ratios than S galaxies ([Graham & Worley 2008](#)).

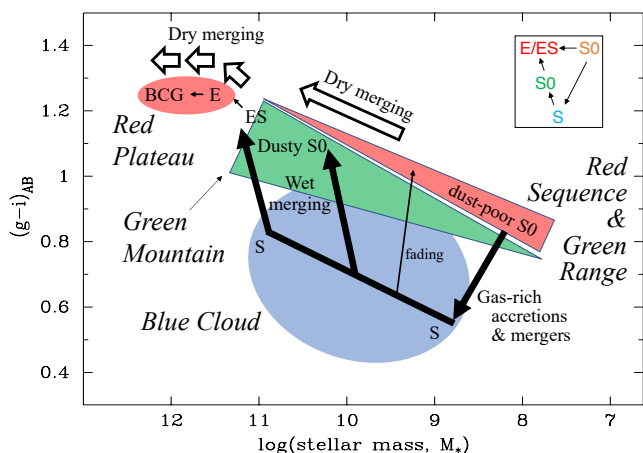


Figure 9. Adaption of the colour-mass schematic shown in [Faber et al. \(2007, their figure 10\)](#). Today’s $z \sim 0$ dust-poor S0 galaxies were once blue, but they need not have ever contained a spiral pattern (fuelled by gas accretion/recycling and induced by gravitational perturbations to their disc). Most S0-to-S transitions have likely already occurred, and this may have happened before the progenitor S0 galaxy became red/green and dust-poor, i.e., the fate of those which did not evolve. The S-to-S0 merger-induced transitions are expected to occur in the past, present, and future. The green side of the ‘red sequence’, or ‘green range’, is due to gas-rich mergers building dust-rich S0 galaxies. These galaxies are an intermediate step on the path to merger-built E galaxies. The ‘fading’ trajectory shown in the figure applies to the past and future migration of blue S galaxies (some stellar mass loss from stellar winds is accounted for). Although not shown, the slope of the red-sequence declines and possibly flattens at masses below 10^7 – $10^8 M_\odot$ (e.g., [de Vaucouleurs & Ables 1968](#); [Roediger et al. 2017](#)). Also not shown is the effect of tidal stripping, which shifts galaxies to the right and potentially upwards. This schematic can be applied to understanding the CMD ([Fig. 5](#)) and the CM_{bhD} ([Fig. 8](#)).

ating S0 galaxies, [Schawinski et al. \(2014\)](#) reported on these two suspected populations in the ‘green valley’: gas-depleted S galaxies²⁷ and S galaxy merger products. [Deeley et al. \(2021\)](#) and others supported this duopoly. Departing from the notion that S0 galaxies are only a bridging population formed from either merged or gas-stripped/starved S galaxies, the ‘Triangal’ recognises a third type of S0 galaxy. It considers the bulk of the ($z = 0$) dust-poor S0 galaxies to be faded S0 (not faded S) galaxies that are predominantly (by stellar mass) primordial.

For dwarf S0 galaxies embedded in a cluster, they tend to be ram-pressure stripped of their gas ([Conselice et al. 2003b](#)), dust-poor ([Bourne et al. 2012](#); [Agius et al. 2015](#)), and red/green. This does not rule out ‘downsizing’ (e.g., [Monaco et al. 2000](#)) or rejuvenation in other environments. If dwarf S0 galaxies are isolated, or still in the periphery of a cluster, they may still have an HI gas reservoir and low levels of current or recent star formation ([di Serego Alighieri et al. 2013](#); [Hallenbeck et al. 2017](#)). The gradual accrual of satellite galaxies and minor mergers will bring new stars and gas and disturb high-angular momentum gas around the central galaxy. The starburst galaxy NGC 3034 (M82; [Mutchler et al. 2007](#), not in sample), with its nascent spiral arms ([Mayya et al. 2005](#)), may be an example of such a transition galaxy. If the galaxies are in

small groups, then this gas may form HI bridges with neighbouring galaxies or robbed of some of its angular momentum through gravitational interactions (with passing galaxies), leading it to fall onto its central galaxy. The extent of any ensuing star formation will dictate how blue, and thus how far into the ‘blue cloud’, the galaxy evolves ([Fig. 9](#)).

The ‘Triangal’ also builds on the phenomenon of S galaxy collisions as a pathway to dust-rich S0 galaxies (e.g., [Deeley et al. 2020, 2021](#); [Coccatto et al. 2022](#)), rather than immediately building E galaxies ([Wright et al. 1990](#)), which require further mergers to reduce/cancel the net angular momentum of the stars and erase the disc(s) in the progenitor galaxies ([Naab & Burkert 2003](#)). The discs of the merger-built S0 galaxies may help preserve the dust clouds, keeping them in orbit over long durations, at least until their dust/gas is removed by, for example, immersion in an X-ray hot halo of gas. The accumulation of dust-rich S0 galaxies at predominantly the *high-mass* end of the S galaxy distribution ([Fig. 5](#)) may reflect the rarity (but not absence) of *low-mass* S galaxy mergers, expected to yield low-mass dust-rich S0 galaxies. This situation may arise in the Virgo Cluster because the high ‘velocity dispersion’ of the galaxies leads to fly-bys rather than collisions for the lower-mass galaxies with less gravitational attraction. Cold gas and dust removal may also be more effective at lower galaxy masses. These evolutionary pathways have been shown schematically in [Fig. 6](#) and [9](#), which builds on [Faber et al. \(2007, their figure 10\)](#) in several ways.

The CMD has long displayed a bimodal distribution (e.g., [Chester & Roberts 1964](#); [Strateva et al. 2001](#); [Faber et al. 2007](#)). Correcting for dust within the external galaxies, as done here, a bimodal distribution in the CMD was also reported by [Cameron et al. \(2009\)](#), and this was also seen using infrared colours ([Alatalo et al. 2014](#)) from the Wide Field Infrared Survey Explorer (WISE; [Wright et al. 2010](#)). The bimodal distribution is also apparent in [Fig. 5](#) and [Fig. 8](#). However, one significant difference here is the notion that spiral galaxies start as spiral-less S0 galaxies.²⁸ The evolutionary chain commenced with what are now the old, metal-poor and dust-poor S0 galaxies in the local Universe. In the younger Universe, these disc galaxies may have either been stripped of their (ability to acquire) gas — and thus effectively experienced a cessation of star formation — or they may have grown through acquisitions, becoming S and more massive S0 galaxies. When these galaxies reside within a hot X-ray-emitting gas cloud, prevalent in galaxy cluster environments, it tends to destroy the dust ([Draine & Salpeter 1979](#)) and prevents gas from cooling to form new stars. With the bulk of their stars old and the galaxy having not experienced major mergers, today’s dust-poor S0 galaxies need never have been S galaxies and are regarded as primordial (ancients, elders) left over from the young Universe. As noted before, they need not all be old, with downsizing and delayed creation capable of producing young(er) discs and even first-generation galaxies from ‘dark galaxies’ (e.g., [O’Neil et al. 2024](#), in preparation; [Soria et al. 2024](#), in preparation).

Another inclusion in [Fig. 9](#) is the explicit production of dust-rich S0 galaxies from major wet mergers. Taken together with the above interpretation of the dust-poor S0 galaxies, this likely contributes to, if not explains, the apparent population of both high- and low-mass S0 galaxies reported by [van den Bergh \(1990\)](#) and

²⁷ As [Peng et al. \(2010\)](#) and others note, the gas may be slowly consumed via dwindling star formation or rapidly removed from the galaxy via various mechanisms.

²⁸ Of course, when they first formed stars, the primordial S0 galaxies would have been blue, and as such, the schema in [Fig. 9](#) does not quite capture that element of the story.

the observations of ETG age reported by van Dokkum & Franx (2001). Due in part to low levels of ongoing star formation (Graham et al. 2023), the dusty S0 galaxies appear on the green side of the ‘red sequence’, referred to here as the ‘green range’. Studying ETGs, Schweizer & Seitzer (1992) revealed that S0 galaxies with signs of merger-induced fine structure tend to reside blueward of the ‘red sequence’ in the CMD. There is also a tendency observed here for dust-rich ETGs to reside on the blue/green side of the ‘red sequence’. These dust-rich S0 galaxies are known merger remnants (Graham 2023b). Hamraz et al. (2019) report that ETGs on the green side of the ‘red sequence’ often show evidence of dust extinction, which they take as a signpost for young stellar populations causing the bluer colours. Conceivably, some of the galaxies reported by Belfiore et al. (2017) to have central low ionisation emission-line regions (cLIERs) may not be spirals with bulges built via secular evolution but lenticulars with merger-built bulges.

Among the sample of 88 ($= 100 - 9 - 3$) Virgo Cluster ETGs (Ferrarese et al. 2006)²⁹ included here, all four dIrr/dE transition objects (VCC 21, VCC 1512, VCC 1499 and VCC 1779) may have weak dust features, and three of these four have relatively blue ($g - i$)_{AB} colours for an ETG. The exception is VCC 1512, which is reported to have $(g - i)_{AB} = 0.99$ mag, although Consolandi et al. (2016) report 0.87 mag. The appearance of star-forming galaxies (Voyer et al. 2014) along the green side of the ‘red sequence’ can also be seen in Roediger et al. (2017, their figure 1). While it is somewhat unclear which of their star-forming galaxies might be S galaxies rather than dusty S0 galaxies, the absence of a ‘blue cloud’ — in their sample of 404 galaxies (Ferrarese et al. 2020) located around Virgo A (aka M87) — suggests few S galaxies are present. In the SFR-mass diagram, the dust-rich S0 galaxies (e.g., NGC 1194, NGC 1316, NGC 5018 and NGC 5128) also contribute toward the well-populated ‘green mountain’, located between the star-forming main sequence and the true E galaxies (Eales et al. 2018a,b; Graham et al. 2023). They are also seen here to shape a ‘green mountain’ in the CMD after correcting their colour for dust, as done for the LTGs.

Differing from Schawinski et al. (2014), these merger-built S0 galaxies tend to be located toward the top of the ‘blue cloud’ of S galaxies. Rather than being a small population that moves rapidly to the ‘red sequence’, they appear to be a substantial population that lingers at the green/red end of the ‘blue cloud’, modulo the adopted correction for dust in these galaxies. This is the opposite behaviour to that concluded by Schawinski et al. (2014). Furthermore, a sample of (potentially) faded S galaxies are located on/near the ‘red sequence’ rather than at the green/red end of the ‘blue cloud’. This, too, is the opposite finding that Schawinski et al. (2014) reached, and it does not depend on a correction for dust in these galaxies. Five dust-poor S0 galaxies (NGC: 1023; 3384; 4371; 4762; and 7332) had previously stood out by overlapping with the S galaxies in the $M_{bh} - M_{*,gal}$ diagram (Fig 1), making them good candidates for faded and transformed S galaxies. *SDSS* colours are available for all but NGC 1023, and they are highlighted in the CMD (Fig. 5). Three are located at the high-mass end of the dust-poor S0 galaxy sequence and have a red colour, while the fourth (NGC 3384) is considered green. Most galaxies in the ‘green valley’ sample of Schaw-

inski et al. (2014) had an unknown morphological type, requiring assumptions about which were faded LTGs or merger-built ETGs, the two migratory scenarios that had been around for decades. The present investigation advocates for a reversal of their conclusions as to the S-to-S0 pathways through the ‘green valley’.

A few lower-mass dust-rich S0 galaxies trace a ‘green range’. This is not a discovery but perhaps a somewhat forgotten observation. The existence of relatively blue E galaxies in the Millennium Galaxy Catalog (MGC) was called out by Driver et al. (2007b) and Cameron et al. (2009). Some of these blue dwarf galaxies (e.g., Moffett et al. 2016, 2019) may be dwarf S0 galaxies, for which the disc was inadvertently missed, rather than actual blue dwarf E galaxies. Related are the blue compact dwarf (BCD) galaxies that are more knotty in structure but also possess an underlying backbone that is a disc (Cairós et al. 2003).

Stars in S galaxies eject metals, and before an S galaxy-collision-induced burst of star formation in the merged system (Mihos et al. 1992), the gas clouds need to cool. This cooling would be associated with the gas-phase metals condensing into dust particles, thus producing dust-obscured starbursts (Calzetti et al. 1994; Mihos & Hernquist 1996; Hopkins et al. 2006). During a collision, the dramatic infall and cooling of gas also produces central accretion discs around black holes and spurs the quasar phenomenon in the disturbed remnant merger products (e.g., Baum & Heckman 1989; Baum et al. 1992; Morse et al. 1998; Kaviraj et al. 2012; Raimundo et al. 2023) and, in some cases, an ultraluminous infrared galaxy (ULIRG; Sanders et al. 1988). This may also be the situation seen by Consolandi et al. (2016, see their figure 10). However, given that S galaxy major merger remnants still have substantial discs, not all of the gas freefalls inward for consumption in a starburst. Substantial amounts of gas and dust remain in place due to their orbital angular momentum. As the AGN fizzles out over time, the S0 merger remnant retains low levels of star formation. The subsequent merger of two or more of these S0 galaxies finally produces a massive E galaxy enshrouded in a hot gas halo that quenches star formation and maintains the red galaxy colour. Low-level radio-mode (as opposed to gas-rich quasar-mode) heating from the central BH, a so-called ‘Benson Burner’³⁰ (Benson et al. 2003; Bower et al. 2006), appears capable of maintaining the hot X-ray gas halo, which keeps the galaxies quenched and red by returning dust to metals in the gas phase and evaporating the cool gas clouds (Ciotti & Ostriker 2001).

Graham et al. (2023) explored if the black hole mass or the M_{bh}/M_* ratio may dictate the SFR of galaxies through AGN feedback (Kauffmann & Haehnelt 2000; Di Matteo et al. 2005; Croton et al. 2006; Cattaneo et al. 2009; Fabian 2012; Cicone et al. 2014). It was found that it did not. Instead, the SFR tracked the galaxy morphology more closely. Thus, the merger/accretion history of galaxies is more relevant than AGN feedback if M_{bh}/M_* is a proxy for such feedback (Terrazas et al. 2016).

5.1 Future Work

Future work could explore the evolution of the metallicity (e.g., Worthey et al. 1992; Chiappini et al. 2003; Schombert & McGaugh 2014), and thus IMF (Calura et al. 2009) due to new generations of stars coming, in part, from mergers. The low-metallicity quasi-primordial dust-poor S0 galaxies (Conselice et al. 2003a; Lisker et al. 2006; Sil’chenko 2013) would have a different IMF to the

²⁹ Among the 16 to 21 Virgo Cluster ETGs which do or may have dust, Ferrarese et al. (2006) suggested that those (2) with strong irregular dust lanes may evolve into those (4) with large (kpc-sized) patchy discs of dust, before settling into those (3) with small (few hundred parsecs), smooth, thin dust discs, i.e., those in the ‘n’ (nuclear) dust bin.

³⁰ Graham & Sahu (2023a, their footnote 33) introduced this term.

dust-rich S0 galaxies built from the merger of S galaxies. A low metallicity would have resulted in the IMF having had a higher fraction of higher-mass stars than forms in S galaxies today (e.g., [Martín-Navarro et al. 2015](#); [Li et al. 2023](#)). The situation is compounded by the mass-metallicity and gas-dust trends observed in disc galaxies today (e.g., [Engelbracht et al. 2008](#); [Mannucci et al. 2010](#)). Along with the galaxies’ internal evolution ([Tan et al. 2014](#)), this can impact the assigned M/L ratios (e.g., [Into & Portinari 2013](#), their figures 5–6). These different populations then find their way into E galaxies, which would have multiple metallicities. As galaxies evolve, one might expect the IMF to change with the B/T ratio and thus velocity dispersion, as observed by, for example, [Spiniello et al. \(2014\)](#); [Smith \(2020\)](#). Following suggestions that a [Salpeter \(1955\)](#) IMF is applicable to ETGs, [Bernardi et al. \(2010](#), their section 5.4) address this IMF issue by respectively adding 0.2 and 0.25 dex (in accord with a [Salpeter \(1955\)](#) IMF) to the masses of their S0 and E galaxies relative to the derivation obtained using a [Chabrier \(2003\)](#) IMF that was maintained for the S galaxies. [Into & Portinari \(2013](#), their table 4) provide zero-point calibrations for the colour-mass relations appropriate for a [Salpeter \(1955\)](#) IMF. Untangling samples of S0 galaxies with different creation histories should be an important next step on this frontier, rather than considering all S0 galaxies have, say, a [Salpeter \(1955\)](#) or diet-Salpeter IMF. IMF gradients and spaxel-by-spaxel variations may also abound (e.g., [Parikh et al. 2018](#); [Martín-Navarro et al. 2023](#)).

For ETGs, it has been suggested that the gravitational potential energy, $\Phi \propto M/R$, correlates better with colour than mass ([Barone et al. 2018](#)), both of which are used in the CMD. However, this is problematic on several fronts. While the virial theorem implies $\sigma^2 \propto M/R$ for a pressure-supported system³¹, S0 galaxies are predominantly rotation-dominated systems, with disc-to-bulge mass ratios substantially greater than 1. As such, the virial theorem does not apply, and using σ^2 to trace the gravitational potential (and $\sigma^2/R_{\text{e,gal}}$ to trace the surface mass density) is only meaningful for the E galaxies. Moreover, even for the true E galaxies, changing R from, say, the radius enclosing 50 per cent of the light to some other percentage will systematically, as a function of the E galaxy’s Sérsic index and thus stellar mass ([Davies et al. 1988](#); [Caon et al. 1993](#)), change the estimated gravitational potential, surface mass density, and implied fraction of dark matter ([Graham 2019a, 2023a](#), fig. A1). More meaningful measures of these quantities for the pressure-supported element of ETGs will come from greater recognition of the multi-component nature of galaxies. Attempts to involve a third parameter (beyond morphology) in the CMD is left for elsewhere.

For the past century, astronomers have frequently overlooked the presence of discs in ordinary ETGs. This is also the case for some (most?) dwarf ETGs, which have been found to rotate (e.g., [Pedraz et al. 2002](#); [Geha et al. 2003](#); [Toloba et al. 2009](#)). Although dwarf S galaxies are uncommon, researchers have discovered weak spiral patterns in some supposed dwarf ETGs ([Jerjen et al. 2000](#); [Barazza et al. 2002](#); [Graham et al. 2003](#)), indicating the existence of discs within these galaxies. Connections in the CMD with dwarf Irregular (dIrr) galaxies and blue compact dwarfs (BCDs) — which also have a disc-like backbone and rotation ([Cairós et al. 2003, 2015](#)) — and rotating low-mass blue/green ETGs ([Driver et al. 2007b](#); [Cameron et al. 2009](#); [Kannappan et al. 2009](#); [Moffett et al. 2019](#)), and dwarf spheroidal galaxies is deferred to else-

where. Nonetheless, for the low-mass (dwarf) galaxies, the role of accretion, mergers and fading, and concepts of primordial versus evolved populations would benefit from further exploration. For instance, are BCDs the product of disc+disc wet major mergers or rejuvenated discs due to lesser accretion events ([Cairós et al. 2001](#), and references therein)? Discs can largely be stripped away from galaxies, leaving behind somewhat naked bulges (aka ‘compact elliptical, cE: [Bekki et al. 2001b](#)), or more violently threshed, leaving behind the tightly bound nuclear star cluster (NSC, aka ‘ultra-compact dwarf, UCD:’ [Bekki et al. 2001a](#)). Investigation of galaxy-morphology-dependent $M_{\text{nsc}}-M_{\text{bh}}$ relations and the $M_{\text{ucd}}-M_{\text{bh}}$ relation ([Graham 2020](#)) will similarly be left for elsewhere. Fig. 1 does not (yet) include dwarf galaxies. However, it suggests that disc-dominated dwarf S0 galaxies may be the place to search for the largely missing population of intermediate-mass black holes ($10^2 < M_{\text{bh}}/M_{\odot} < 10^5$).

Future studies of the CMD may also benefit from introducing the wealth of additional morphological information, such as spiral strength and bar strength, as meticulously catalogued in the RC3 ([de Vaucouleurs et al. 1991](#)) and elsewhere (e.g., [Buta et al. 2015](#)). For instance, it is noted here that the dust-poor S0 galaxies tend not to be S0⁺ galaxies but S0⁰ or S0⁻, while the dust-rich S0 galaxies can be S0⁻, S0⁰ and S0⁺.

6 SUMMARY

This paper paints morphologies into the CMD and colour-codes ETGs based on their dust content. Doing so has better revealed the substructure in the CMD. Rather than just ETGs (no spiral pattern) versus LTGs (contains a spiral pattern), three types of S0 galaxy are considered: dust-poor primordial S0 (not assumed to have once had a spiral pattern), dust-poor S0 (from faded S), and wet-merger built dust-rich S0 galaxies. Progress with, and new detail in, the $M_{\text{bh}}-M_{*,\text{sph}}$ diagram (Fig. 1) has aided adjustments of interpretation in the CMD, including the notion of a buried ‘green mountain’ of merger-built dust-rich S0 galaxies.

Within the CMD, the ‘blue cloud’ would have been the dominant feature in the early Gyrs of the Universe, with some galaxy discs forming spiral patterns that survived until today and others neither able to sustain nor obtain one. Those unable to have a spiral flourish will have fallen out of the ‘blue cloud’, but this does not mean they once possessed a spiral pattern. While much work is focussed on the future evolution of today’s S galaxies by trying to shift them onto the ‘red sequence’, less attention (but see [Bravo et al. 2022](#)) seems to have been paid to the past evolution of spiral-less disc galaxies. Here, the evolutionary sequence known as the ‘Triangal’ (Fig. 2) is mapped into the CMD (Fig. 6 and 9), revealing how S galaxies can be a bridging population between what are today’s dust-poor and dust-rich S0 galaxies, as observed in the $M_{\text{bh}}-M_{*,\text{sph}}$ diagram (Fig. 1).

This paper introduces and checks the compatibility and applicability of a revised schema which builds on the galaxy evolutionary tracks in the CMD presented by [Faber et al. \(2007\)](#) and other works. It shows the Tuning Fork morphology sequence (S - S0 - E) in the CMD (e.g., [Quilley & de Lapparent 2022](#)) and expands on this to reveal the pathways captured by the ‘Triangal’ ([Graham 2023c](#)). This includes S0 (now dust-poor) \rightarrow S \rightarrow S0 (dust-rich) \rightarrow ES/E, encapsulating the concept that spiral patterns likely emerged in spiral-less lenticular galaxies due to internal instabilities or perturbations from giant molecular clouds or external perturbations from gas accretion and minor mergers ([Toomre 1977](#)). This path-

³¹ The quantity σ is typically, albeit incorrectly, taken as the luminosity-weighted line of sight velocity dispersion within R .

way was addressed by Kannappan et al. (2009) in terms of blue S0 galaxies at low masses. Fig. 1 captures this and the major wet merger-induced transition from S galaxy to dust-rich S0 galaxy — for which the turbulence in the new disc will be higher than in the S galaxies and the velocity dispersion elevated. Past mergers of what are today’s dust-poor S0 galaxies (which were once star-forming galaxies) can also yield massive S0 galaxies, and it has been suggested that this may explain compact massive galaxies³² (Graham & Sahu 2023b). Additional mergers of dust-rich S0 galaxies will further erode their discs to produce spheroid-dominated ES and E galaxies, as seen in Fig. 1. This provides a more nuanced scenario than envisioned by a statement like ‘disc galaxy mergers produce E galaxies’. It also departs from the notion of a single Hubble type for S0 galaxies and from de Vaucouleurs’ T-types confining all S0 galaxies to a bridging population between S and E galaxies, which is the main paradigm shift of the ‘Triangal’.

Here, the single ‘red sequence’ is better regarded as two sequences: one for (predominantly primordial) dust-poor S0 galaxies yielding the sloping component of the ‘red sequence’ and a ‘red plateau’ defined by (pure) E galaxies built via dry major mergers. These E galaxies account for the previously seen levelling off of colour in the distribution at high masses in the CMD (e.g., de Vaucouleurs & Ables 1968; Jiménez et al. 2011). New in regard to this is the clearer separation of galaxy types, facilitated by careful multi-component decompositions of the galaxy light.

The appearance of the ‘Triangal’ in the CMD, as shown here for the first time, readily maps into the $CM_{bh}D$. The ‘Triangal’ serves as context for building on the apparent red and blue sequences in the $M_{bh}-M_*$ diagram (Savorgnan et al. 2016) and the M_{bh} -colour diagram (Dullo et al. 2020). In Section 4.3, (i) the designation of galaxy type in the M_{bh} -colour diagram is expanded beyond simply LTG versus ETG and dust corrections are applied to LTGs and ETGs with dust-rich discs. This redefines the blue sequence in the M_{bh} -colour diagram by incorporating the dust-rich S0 galaxies with the S galaxies, and it redefines the ‘red sequence’ in the M_{bh} -colour diagram due to galaxy-type-awareness, with a plateau evident for the (discless) E galaxies. Finally, it also enables one to better understand the M_{bh} -colour relations in terms of galaxy evolution.

ACKNOWLEDGEMENTS

The author is grateful for past conversations regarding galaxy colours with his initial PhD supervisor, Natarajan (Vis) Visvanathan (Faulkner 2002). This work is based partly on observations made with the Spitzer Space Telescope, which was operated by the Jet Propulsion Laboratory, California Institute of Technology, under a contract with NASA. This work has also used the NASA/IPAC Infrared Science Archive (IRSA) and the NASA/IPAC Extragalactic Database (NED), funded by NASA and operated by the California Institute of Technology. This research has used the NASA/SAO Astrophysics Data System Bibliographic Services. It is also based partly on observations made with the NASA/ESA Hubble Space Telescope, obtained from the Mikulski Archive for Space Telescopes and the Hubble Legacy Archive. Funding for SDSS-III has been provided by the Alfred P. Sloan Foundation, the Participating Institutions, the National Science Foundation, and the U.S. Department of Energy Office of Science.

³² Some ‘compact elliptical’ (cE) dwarf galaxies may instead be the bulges of heavily disc-stripped galaxies (Bekki et al. 2001b; Graham 2013).

7 DATA AVAILABILITY

The data used for this article are available in the references provided. The S⁴G dataset Digital Object Identifier (DOI) is 10.26131/IRSA425.

REFERENCES

- Agius N. K., et al., 2015, *MNRAS*, **451**, 3815
Aguerri J. A. L., Muñoz-Tuñón C., Varela A. M., Prieto M., 2000, *A&A*, **361**, 841
Alatalo K., Cales S. L., Appleton P. N., Kewley L. J., Lacy M., Lisenfeld U., Nyland K., Rich J. A., 2014, *ApJ*, **794**, L13
Alcock C., et al., 2000, *ApJ*, **542**, 281
Alexander S., 1852, *AJ*, **2**, 97
Andredakis Y. C., Peletier R. F., Balcells M., 1995, *MNRAS*, **275**, 874
Ansel’ m A. A., et al., 1998, *Uspekhi Fizicheskikh Nauk*, **41**, 407
Aragón-Salamanca A., Bedregal A. G., Merrifield M. R., 2006, *A&A*, **458**, 101
Arnold J. A., Romanowsky A. J., Brodie J. P., Chomiuk L., Spitler L. R., Strader J., Benson A. J., Forbes D. A., 2011, *ApJ*, **736**, L26
Azimov Y. I., 2016, *International Journal of Modern Physics A*, **31**, 1645004
Baade W., Minkowski R., 1954, *ApJ*, **119**, 206
Baes M., et al., 2014, *MNRAS*, **444**, L90
Bait O., Barway S., Wadadekar Y., 2017, *MNRAS*, **471**, 2687
Balcells M., Graham A. W., Peletier R. F., 2007, *ApJ*, **665**, 1084
Baldwin J. E., Elsmore B., 1954, *Nature*, **173**, 818
Barazza F. D., Binggeli B., Jerjen H., 2002, *A&A*, **391**, 823
Barnes J. E., Hernquist L., 1996, *ApJ*, **471**, 115
Barone T. M., et al., 2018, *ApJ*, **856**, 64
Barr J. M., Bedregal A. G., Aragón-Salamanca A., Merrifield M. R., Bamford S. P., 2007, *A&A*, **470**, 173
Barway S., Wadadekar Y., Kembhavi A. K., Mayya Y. D., 2009, *MNRAS*, **394**, 1991
Bassett R., Bekki K., Cortese L., Couch W., 2017, *MNRAS*, **471**, 1892
Baum W. A., 1959, *PASP*, **71**, 106
Baum S. A., Heckman T., 1989, *ApJ*, **336**, 681
Baum S. A., Heckman T. M., van Breugel W., 1992, *ApJ*, **389**, 208
Bekenstein J. D., 1973, *Phys. Rev. D*, **7**, 2333
Bekki K., Couch W. J., Drinkwater M. J., 2001a, *ApJ*, **552**, L105
Bekki K., Couch W. J., Drinkwater M. J., Gregg M. D., 2001b, *ApJ*, **557**, L39
Bekki K., Couch W. J., Shioya Y., 2002, *ApJ*, **577**, 651
Belfiore F., et al., 2017, *MNRAS*, **466**, 2570
Bell E. F., de Jong R. S., 2001, *ApJ*, **550**, 212
Bell E. F., McIntosh D. H., Katz N., Weinberg M. D., 2003, *ApJS*, **149**, 289
Bellstedt S., Graham A. W., Forbes D. A., Romanowsky A. J., Brodie J. P., Strader J., 2017, *MNRAS*, **470**, 1321
Bender R., 1988, *A&A*, **193**, L7
Benson A. J., Bower R. G., Frenk C. S., Lacey C. G., Baugh C. M., Cole S., 2003, *ApJ*, **599**, 38
Bernardi M., Shankar F., Hyde J. B., Mei S., Marulli F., Sheth R. K., 2010, *MNRAS*, **404**, 2087
Bertin G., Lin C. C., eds, 1996, *Spiral structure in galaxies a density wave theory*. Cambridge, MA MIT Press
Bertola F., Galletta G., Kotanyi C., Zeilinger W. W., 1988a, *MNRAS*, **234**, 733
Bertola F., Buson L. M., Zeilinger W. W., 1988b, *Nature*, **335**, 705
Bizyaev D. V., Kautsch S. J., Mosenkov A. V., Reshetnikov V. P., Sotnikova N. Y., Yablokova N. V., Hillyer R. W., 2014, *ApJ*, **787**, 24
Böker T., Laine S., van der Marel R. P., Sarzi M., Rix H.-W., Ho L. C., Shields J. C., 2002, *AJ*, **123**, 1389
Bond J. R., Szalay A. S., Turner M. S., 1982, *Phys. Rev. Lett.*, **48**, 1636
Boselli A., Gavazzi G., 2014, *A&ARv*, **22**, 74
Boselli A., Boissier S., Cortese L., Gavazzi G., 2008, *ApJ*, **674**, 742
Bourne N., et al., 2012, *MNRAS*, **421**, 3027

- Bower R. G., Lucey J. R., Ellis R. S., 1992, *MNRAS*, **254**, 601
- Bower R. G., Benson A. J., Malbon R., Helly J. C., Frenk C. S., Baugh C. M., Cole S., Lacey C. G., 2006, *MNRAS*, **370**, 645
- Brammer G. B., et al., 2009, *ApJ*, **706**, L173
- Bravo M., Robotham A. S. G., Lagos C. d. P., Davies L. J. M., Bellstedt S., Thorne J. E., 2022, *MNRAS*, **511**, 5405
- Bremer M. N., et al., 2018, *MNRAS*, **476**, 12
- Burstein D., Ho L. C., Huchra J. P., Macri L. M., 2005, *ApJ*, **621**, 246
- Buta R. J., et al., 2015, *ApJS*, **217**, 32
- Cairós L. M., Vílchez J. M., González Pérez J. N., Iglesias-Páramo J., Caon N., 2001, *ApJS*, **133**, 321
- Cairós L. M., Caon N., Papaderos P., Noeske K., Vílchez J. M., García Lorenzo B., Muñoz-Tuñón C., 2003, *ApJ*, **593**, 312
- Cairós L. M., Caon N., Weilbacher P. M., 2015, *A&A*, **577**, A21
- Caldwell N., Rose J. A., Concannon K. D., 2003, *AJ*, **125**, 2891
- Calura F., Pipino A., Chiappini C., Matteucci F., Maiolino R., 2009, *A&A*, **504**, 373
- Calzetti D., Kinney A. L., Storchi-Bergmann T., 1994, *ApJ*, **429**, 582
- Cameron E., Driver S. P., Graham A. W., Liske J., 2009, *ApJ*, **699**, 105
- Caon N., Capaccioli M., D’Onofrio M., 1993, *MNRAS*, **265**, 1013
- Capaccioli M., Caon N., 1992, in Longo G., Capaccioli M., Busarello G., eds, *Astrophysics and Space Science Library Vol. 178, Morphological and Physical Classification of Galaxies*. p. 99, doi:10.1007/978-94-011-2522-2_8
- Cappellari M., et al., 2011, *MNRAS*, **416**, 1680
- Carignan C., Freeman K. C., 1988, *ApJ*, **332**, L33
- Carr B. J., Hawking S. W., 1974, *MNRAS*, **168**, 399
- Carr B., Kühnel F., 2020, *Annual Review of Nuclear and Particle Science*, **70**, 355
- Carter D., 1978, *MNRAS*, **182**, 797
- Cattaneo A., et al., 2009, *Nature*, **460**, 213
- Chabrier G., 2003, *ApJ*, **586**, L133
- Chester C., Roberts M. S., 1964, *AJ*, **69**, 635
- Chiappini C., Romano D., Matteucci F., 2003, *MNRAS*, **339**, 63
- Ciambur B. C., 2015, *ApJ*, **810**, 120
- Ciambur B. C., Graham A. W., 2016, *MNRAS*, **459**, 1276
- Cicone C., et al., 2014, *A&A*, **562**, A21
- Ciotti L., Ostriker J. P., 2001, *ApJ*, **551**, 131
- Ciotti L., D’Ercole A., Pellegrini S., Renzini A., 1991, *ApJ*, **376**, 380
- Coccatto L., Fraser-McKelvie A., Jaffé Y. L., Johnston E. J., Cortesi A., Pallero D., 2022, *MNRAS*, **515**, 201
- Common A. A., 1883, *MNRAS*, **43**, 255
- Conselice C. J., 2002, *ApJ*, **573**, L5
- Conselice C. J., Gallagher John S. I., Wyse R. F. G., 2003a, *AJ*, **125**, 66
- Conselice C. J., O’Neil K., Gallagher J. S., Wyse R. F. G., 2003b, *ApJ*, **591**, 167
- Conselice C. J., Wilkinson A., Duncan K., Mortlock A., 2016, *ApJ*, **830**, 83
- Consolandi G., Gavazzi G., Fumagalli M., Dotti M., Fossati M., 2016, *A&A*, **591**, A38
- Costantin L., et al., 2023, *Nature*, **623**, 499
- Côté P., et al., 2004, *ApJS*, **153**, 223
- Croton D. J., et al., 2006, *MNRAS*, **365**, 11
- Curtis H. D., 1918, *Publications of Lick Observatory*, **13**, 9
- D’Onghia E., Vogelsberger M., Hernquist L., 2013, *ApJ*, **766**, 34
- Daddi E., et al., 2005, *ApJ*, **626**, 680
- Damjanov I., et al., 2009, *ApJ*, **695**, 101
- Davies R. D., Lewis B. M., 1973, *MNRAS*, **165**, 231
- Davies J. I., Phillips S., Cawson M. G. M., Disney M. J., Kibblewhite E. J., 1988, *MNRAS*, **232**, 239
- Davis B. L., Graham A. W., Seigar M. S., 2017, *MNRAS*, **471**, 2187
- Davis B. L., Graham A. W., Cameron E., 2019, *ApJ*, **873**, 85
- De Looze I., et al., 2013, *MNRAS*, **436**, 1057
- Deeley S., et al., 2020, *MNRAS*, **498**, 2372
- Deeley S., Drinkwater M. J., Sweet S. M., Bekki K., Couch W. J., Forbes D. A., Dolfi A., 2021, *MNRAS*, **508**, 895
- Di Matteo T., Springel V., Hernquist L., 2005, *Nature*, **433**, 604
- Dokshitzer Y. L., 1998, Vladimir Gribov (BH) (arXiv:physics/9801025), <https://arxiv.org/abs/physics/9801025v1>
- Draine B. T., Salpeter E. E., 1979, *ApJ*, **231**, 77
- Draper H., 1882, *MNRAS*, **42**, 367
- Dressler A., Richstone D. O., 1988, *ApJ*, **324**, 701
- Dreyer J. L. E., 1888, *Mem. RAS*, **49**, 1
- Dreyer J. L. E., 1895, *Mem. RAS*, **51**, 185
- Dreyer J. L. E., 1910, *Mem. RAS*, **59**, 105
- Driver S. P., Popescu C. C., Tuffs R. J., Liske J., Graham A. W., Allen P. D., de Propriis R., 2007a, *MNRAS*, **379**, 1022
- Driver S. P., Allen P. D., Liske J., Graham A. W., 2007b, *ApJ*, **657**, L85
- Driver S. P., Popescu C. C., Tuffs R. J., Graham A. W., Liske J., Baldry I., 2008, *ApJ*, **678**, L101
- Dullo B. T., Graham A. W., 2014, *MNRAS*, **444**, 2700
- Dullo B. T., Bouquin A. Y. K., Gil de Paz A., Knapen J. H., Gorgas J., 2020, *ApJ*, **898**, 83
- Eales S., et al., 2018a, *MNRAS*, **473**, 3507
- Eales S. A., et al., 2018b, *MNRAS*, **481**, 1183
- Ebnetter K., Djorgovski S., Davis M., 1988, *AJ*, **95**, 422
- Elmegreen D. M., Elmegreen B. G., 1987, *ApJ*, **314**, 3
- Engelbracht C. W., Rieke G. H., Gordon K. D., Smith J. D. T., Werner M. W., Moustakas J., Willmer C. N. A., Vanzi L., 2008, *ApJ*, **678**, 804
- Event Horizon Telescope Collaboration et al., 2019, *ApJ*, **875**, L4
- Faber S. M., et al., 2007, *ApJ*, **665**, 265
- Fabian A. C., 2012, *ARA&A*, **50**, 455
- Fall S. M., 1983, in Athanassoula E., ed., *IAU Symposium Vol. 100, Internal Kinematics and Dynamics of Galaxies*. pp 391–398
- Fall S. M., Efstathiou G., 1980, *MNRAS*, **193**, 189
- Farouki R., Shapiro S. L., 1981, *ApJ*, **243**, 32
- Faulkner D. J., 2002, *BAAS*, **34**, 1386
- Fazio G. G., et al., 2004, *ApJS*, **154**, 10
- Ferrarese L., et al., 2006, *ApJS*, **164**, 334
- Ferrarese L., et al., 2020, *ApJ*, **890**, 128
- Frenk C. S., White S. D. M., Efstathiou G., Davis M., 1985, *Nature*, **317**, 595
- Fukuda Y., et al., 1999, *Phys. Rev. Lett.*, **82**, 2644
- Gavazzi G., Boselli A., Donati A., Franzetti P., Scodreggio M., 2003, *A&A*, **400**, 451
- Geha M., Guhathakurta P., van der Marel R. P., 2003, *AJ*, **126**, 1794
- Geisler D., Lee M. G., Kim E., 1996, *AJ*, **111**, 1529
- Genzel R., Thatte N., Krabbe A., Kroker H., Tacconi-Garman L. E., 1996, *ApJ*, **472**, 153
- Genzel R., Eckart A., Ott T., Eisenhauer F., 1997, *MNRAS*, **291**, 219
- Gerhard O. E., 1981, *MNRAS*, **197**, 179
- Ghez A. M., Klein B. L., Morris M., Becklin E. E., 1998, *ApJ*, **509**, 678
- Gorbachev V. I., 1970, *Soviet Ast.*, **14**, 182
- Goudfrooij P., Norgaard-Nielsen H. U., Hansen L., Jorgensen H. E., de Jong T., 1990, *A&A*, **228**, L9
- Graham A. W., 2001, *AJ*, **121**, 820
- Graham A. W., 2012, *ApJ*, **746**, 113
- Graham A. W., 2013, in Oswald T. D., Keel W. C., eds., *Planets, Stars and Stellar Systems. Volume 6: Extragalactic Astronomy and Cosmology*. Springer Science+Business Media, Dordrecht, pp 91–140, doi:10.1007/978-94-007-5609-0_2
- Graham A. W., 2016, in Laurikainen E., Peletier R., Gadotti D., eds, *Astrophysics and Space Science Library Vol. 418, Galactic Bulges*. p. 263 (arXiv:1501.02937), doi:10.1007/978-3-319-19378-6_11
- Graham A. W., 2019a, *Publ. Astron. Soc. Australia*, **36**, e035
- Graham A. W., 2019b, *MNRAS*, **487**, 4995
- Graham A. W., 2020, *MNRAS*, **492**, 3263
- Graham A. W., 2023a, *MNRAS*, **518**, 6293
- Graham A. W., 2023b, *MNRAS*, **521**, 1023
- Graham A. W., 2023c, *MNRAS*, **522**, 3588
- Graham A. W., Guzmán R., 2003, *AJ*, **125**, 2936
- Graham A. W., Sahu N., 2023a, *MNRAS*, **518**, 2177
- Graham A. W., Sahu N., 2023b, *MNRAS*, **520**, 1975
- Graham A. W., Scott N., 2013, *ApJ*, **764**, 151
- Graham A. W., Worley C. C., 2008, *MNRAS*, **388**, 1708
- Graham A. W., Jerjen H., Guzmán R., 2003, *AJ*, **126**, 1787

- Graham A. W., Ciambur B. C., Savorgnan G. A. D., 2016, *ApJ*, **831**, 132
- Graham A. W., Janz J., Penny S. J., Chilingarian I. V., Ciambur B. C., Forbes D. A., Davies R. L., 2017, *ApJ*, **840**, 68
- Graham A. W., Soria R., Davis B. L., 2019, *MNRAS*, **484**, 814
- Graham A. W., Jarrett T., M.E. C., 2023, *MNRAS*, submitted
- Grisaru M. T., Pendleton H. N., van Nieuwenhuizen P., 1977, *Phys. Rev. D*, **15**, 996
- Gunn J. E., Gott J. Richard I., 1972, *ApJ*, **176**, 1
- Haehnelt M. G., Rees M. J., 1993, *MNRAS*, **263**, 168
- Hallenbeck G., Koopmann R., Giovanelli R., Haynes M. P., Huang S., Leisman L., Papastergis E., 2017, *AJ*, **154**, 58
- Hamraz E., Peletier R. F., Khosroshahi H. G., Valentijn E. A., den Brok M., Venhola A., 2019, *A&A*, **625**, A94
- Hart R., Berendzen R., 1971, *Journal for the History of Astronomy*, **2**, 109
- Hau G. K. T., Bower R. G., Kilborn V., Forbes D. A., Balogh M. L., Oosterloo T., 2008, *MNRAS*, **385**, 1965
- Häußler B., et al., 2022, *A&A*, **664**, A92
- Hawking S., 1971, *MNRAS*, **152**, 75
- Hawking S. W., 1974, *Nature*, **248**, 30
- Hawking S. W., 1975, *Communications in Mathematical Physics*, **43**, 199
- Hernquist L., 1993, *ApJ*, **409**, 548
- Herschel W., 1786, *Philosophical Transactions of the Royal Society of London Series I*, **76**, 457
- Herschel W., 1789, *Philosophical Transactions of the Royal Society of London Series I*, **79**, 212
- Herschel W., 1802, *Philosophical Transactions of the Royal Society of London Series I*, **92**, 477
- Herschel J. F. W., 1864, *Philosophical Transactions of the Royal Society of London Series I*, **154**, 1
- Hertzsprung E., 1911, *Publikationen des Astrophysikalischen Observatoriums zu Potsdam*, **22**, A1
- Hopkins P. F., Hernquist L., Cox T. J., Di Matteo T., Robertson B., Springel V., 2006, *ApJS*, **163**, 1
- Hubble E. P., 1926, *ApJ*, **64**, 321
- Hubble E. P., 1936, *Realm of the Nebulae*. New Haven: Yale University Press
- Huggins W., 1882, *Nature*, **25**, 489
- Illingworth G. D., et al., 2013, *ApJS*, **209**, 6
- Into T., Portinari L., 2013, *MNRAS*, **430**, 2715
- Irwin J. A., Stil J. M., Bridges T. J., 2001, *MNRAS*, **328**, 359
- Jeans J. H., 1919, *Problems of cosmogony and stellar dynamics*. Cambridge Univ. Press, Cambridge
- Jeans J. H., 1928, *Astronomy and cosmogony*. Cambridge: Cambridge University Press
- Jerjen H., Kalnajs A., Binggeli B., 2000, *A&A*, **358**, 845
- Jiménez N., Cora S. A., Bassino L. P., Tecce T. E., Smith Castelli A. V., 2011, *MNRAS*, **417**, 785
- Julian W. H., Toomre A., 1966, *ApJ*, **146**, 810
- Kannappan S. J., Guie J. M., Baker A. J., 2009, *AJ*, **138**, 579
- Kant I., 1755, *Allgemeine Naturgeschichte und Theorie des Himmels* (in German). Universal Natural History and Theory of the Heavens (p.367). Königsberg, Germany. Translated by Stephen Palmquist in Kant's *Critical Religion* (in 2000). Ashgate, Aldershot, p.320
- Kauffmann G., Haehnelt M., 2000, *MNRAS*, **311**, 576
- Kauffmann G., White S. D. M., Guiderdoni B., 1993, *MNRAS*, **264**, 201
- Kaviraj S., et al., 2012, *MNRAS*, **423**, 49
- Kazantzidis S., Łokas E. L., Mayer L., Knebe A., Klimentowski J., 2011, *ApJ*, **740**, L24
- Keeler J. E., 1899, *MNRAS*, **60**, 128
- Keeler J. E., 1900, *ApJ*, **11**, 325
- Kelvin L. S., et al., 2018, *MNRAS*, **477**, 4116
- Kennedy R., et al., 2016, *MNRAS*, **460**, 3458
- Kenney J. D. P., Koopmann R. A., 1999, *AJ*, **117**, 181
- Kennicutt Robert C. J., Skillman E. D., 2001, *AJ*, **121**, 1461
- Khalatyan A., Cattaneo A., Schramm M., Gottlöber S., Steinmetz M., Wisotzki L., 2008, *MNRAS*, **387**, 13
- Khosroshahi H. G., Wadadekar Y., Kembhavi A., 2000, *ApJ*, **533**, 162
- Kodama T., Arimoto N., 1997, *A&A*, **320**, 41
- Kormendy J., Bender R., 1996, *ApJ*, **464**, L119
- Kormendy J., Ho L. C., 2013, *ARA&A*, **51**, 511
- Kroupa P., 1998, in Rebolo R., Martin E. L., Zapatero Osorio M. R., eds, *Astronomical Society of the Pacific Conference Series Vol. 134, Brown Dwarfs and Extrasolar Planets*. p. 483
- Kroupa P., 2002, *Science*, **295**, 82
- Laplace P. S., 1796, *Exposition du Système du monde*. Cercie-Social, Paris. Exposition of the System of the World, translated from French by J. Pond (London: R. Philips, 1809)
- Laplace P. S., 1799-1825, *Mécanique Céleste*. Vols 1-5. Duprat, Paris
- Laurikainen E., Salo H., Buta R., Knapen J. H., 2007, *MNRAS*, **381**, 401
- Li J., Liu C., Zhang Z.-Y., Tian H., Fu X., Li J., Yan Z.-Q., 2023, *Nature*, **613**, 460
- Liller M. H., 1966, *ApJ*, **146**, 28
- Lilly S. J., Carollo C. M., Pipino A., Renzini A., Peng Y., 2013, *ApJ*, **772**, 119
- Lin C. C., Shu F. H., 1964, *ApJ*, **140**, 646
- Lipatov L., 1999, *Surveys in High Energy Physics*, **14**, 1
- Lisker T., Glatt K., Westera P., Grebel E. K., 2006, *AJ*, **132**, 2432
- Lisker T., Grebel E. K., Binggeli B., 2008, *AJ*, **135**, 380
- López-Sánchez Á. R., Koribalski B. S., van Eymeren J., Esteban C., Kirby E., Jerjen H., Lonsdale N., 2012, *MNRAS*, **419**, 1051
- Lundmark K., 1925, *MNRAS*, **85**, 865
- Lundmark K., 1927, *Nova Acta Regiae Soc. Sci. Upsaliensis Ser. V*, pp 1–127
- Lundmark K., 1956, *Vistas in Astronomy*, **2**, 1607
- MacArthur L. A., González J. J., Courteau S., 2009, *MNRAS*, **395**, 28
- Maddison R., 2011, *The Antiquarian Astronomer*, **5**, 36
- Mannucci F., Cresci G., Maiolino R., Marconi A., Gnerucci A., 2010, *MNRAS*, **408**, 2115
- Mapelli M., 2015, *Galaxies*, **3**, 192
- Mapelli M., Rampazzo R., Marino A., 2015, *A&A*, **575**, A16
- Marcum P. M., Aars C. E., Fanelli M. N., 2004, *AJ*, **127**, 3213
- Martín-Navarro I., et al., 2015, *ApJ*, **806**, L31
- Martín-Navarro I., et al., 2023, *arXiv e-prints*, p. arXiv:2312.13355
- Martin D. C., et al., 2007, *ApJS*, **173**, 342
- Mayya Y. D., Carrasco L., Luna A., 2005, *ApJ*, **628**, L33
- Mazzarella J. M., Bothun G. D., Boroson T. A., 1991, *AJ*, **101**, 2034
- Meidt S. E., et al., 2014, *ApJ*, **788**, 144
- Michard R., 1984, *A&A*, **140**, L39
- Mihos J. C., Hernquist L., 1996, *ApJ*, **464**, 641
- Mihos J. C., Richstone D. O., Bothun G. D., 1992, *ApJ*, **400**, 153
- Minkowski R., Aller L. H., 1954, *ApJ*, **119**, 232
- Miyoshi M., Moran J., Herrnstein J., Greenhill L., Nakai N., Diamond P., Inoue M., 1995, *Nature*, **373**, 127
- Moffett A. J., et al., 2016, *MNRAS*, **457**, 1308
- Moffett A. J., et al., 2019, *MNRAS*, **489**, 2830
- Möllenhoff C., 2004, *A&A*, **415**, 63
- Monaco P., Salucci P., Danese L., 2000, *MNRAS*, **311**, 279
- Moore B., Katz N., Lake G., Dressler A., Oemler A., 1996, *Nature*, **379**, 613
- Morrissey P., et al., 2007, *ApJS*, **173**, 682
- Morse J. A., Cecil G., Wilson A. S., Tsvetanov Z. I., 1998, *ApJ*, **505**, 159
- Mutchler M., et al., 2007, *PASP*, **119**, 1
- Naab T., Burkert A., 2003, *ApJ*, **597**, 893
- Navarro J. F., White S. D. M., 1994, *MNRAS*, **267**, 401
- Negroponte J., White S. D. M., 1983, *MNRAS*, **205**, 1009
- Nieto J. L., Capaccioli M., Held E. V., 1988, *A&A*, **195**, L1
- Ohta K., Hamabe M., Wakamatsu K.-I., 1990, *ApJ*, **357**, 71
- Olive K. A., Schramm D. N., Steigman G., Turner M. S., Yang J., 1981, *ApJ*, **246**, 557
- Padilla N. D., Strauss M. A., 2008, *MNRAS*, **388**, 1321
- Pagels H., Primack J. R., 1982, *Phys. Rev. Lett.*, **48**, 223
- Parikh T., et al., 2018, *MNRAS*, **477**, 3954
- Park J.-H., Lee Y.-W., 1997, *ApJ*, **476**, 28
- Parsons W., 1861, *Philosophical Transactions of the Royal Society of London*, **151**, 681
- Parsons L., 1878, *Scientific Transactions of the Royal Dublin Society*, **II**

- Paudel S., Lisker T., Kuntschner H., Grebel E. K., Glatt K., 2010, *MNRAS*, **405**, 800
- Pawlik A. H., Milosavljević M., Bromm V., 2011, *ApJ*, **731**, 54
- Pedraz S., Gorgas J., Cardiel N., Sánchez-Blázquez P., Guzmán R., 2002, *MNRAS*, **332**, L59
- Peletier R. F., Balcells M., 1996, *AJ*, **111**, 2238
- Peng Y.-j., Renzini A., 2020, *MNRAS*, **491**, L51
- Peng Y.-j., et al., 2010, *ApJ*, **721**, 193
- Perrine C. D., 1904, *Lick Observatory Bulletin*, **64**, 47
- Pickering E. C., 1890, *Annals of Harvard College Observatory*, **18**, 113
- Prieto M., Gottesman S. T., Aguerri J.-A. L., Varela A.-M., 1997, *AJ*, **114**, 1413
- Prieto J., Jimenez R., Haiman Z., 2013, *MNRAS*, **436**, 2301
- Quilley L., de Lapparent V., 2022, *A&A*, **666**, A170
- Raimundo S. I., Malkan M., Vestergaard M., 2023, *Nature Astronomy*, **7**, 463
- Rakos K., Schombert J., 2004, *AJ*, **127**, 1502
- Rampazzo R., et al., 2007, *MNRAS*, **381**, 245
- Randall S. W., Markevitch M., Clowe D., Gonzalez A. H., Bradač M., 2008, *ApJ*, **679**, 1173
- Rarita W., Schwinger J., 1941, *Physical Review*, **60**, 61
- Rathore H., Kumar K., Mishra P. K., Wadadekar Y., Bait O., 2022, *MNRAS*, **513**, 389
- Rest A., van den Bosch F. C., Jaffe W., Tran H., Tsvetanov Z., Ford H. C., Davies J., Schafer J., 2001, *AJ*, **121**, 2431
- Reynolds J. H., 1920a, *MNRAS*, **80**, 746
- Reynolds J. H., 1920b, *MNRAS*, **81**, 129
- Reynolds J. H., 1925, *MNRAS*, **85**, 1014
- Reynolds J. H., 1927, *The Observatory*, **50**, 185
- Rizzo F., Fraternali F., Iorio G., 2018, *MNRAS*, **476**, 2137
- Roberts I., 1893, *A Selection of Photographs of Stars, Star-Clusters and Nebulae, together with Information concerning the Instruments and the Methods employed in the pursuit of Celestial Photography*. The Universal Press, London
- Roberts I., 1895, *MNRAS*, **56**, 70
- Robertson B. E., Bullock J. S., 2008, *ApJ*, **685**, L27
- Roediger J. C., Courteau S., 2015, *MNRAS*, **452**, 3209
- Roediger J. C., et al., 2017, *ApJ*, **836**, 120
- Romanowsky A. J., Fall S. M., 2012, *ApJS*, **203**, 17
- Romeo A. D., Napolitano N. R., Covone G., Sommer-Larsen J., Antonuccio-Delogu V., Capaccioli M., 2008, *MNRAS*, **389**, 13
- Roos N., Norman C. A., 1979, *A&A*, **76**, 75
- Rosse T. E. O., 1850, *Philosophical Transactions of the Royal Society of London Series I*, **140**, 499
- Russell H. N., 1914, *Popular Astronomy*, **22**, 275
- Saglia R. P., et al., 2016, *ApJ*, **818**, 47
- Saha K., Cortesi A., 2018, *ApJ*, **862**, L12
- Sahu N., Graham A. W., Davis B. L., 2019a, *ApJ*, **876**, 155
- Sahu N., Graham A. W., Davis B. L., 2019b, *ApJ*, **887**, 10
- Sahu N., Graham A. W., Hon D. S. H., 2023, *MNRAS*, **518**, 1352
- Salim S., 2014, *Serbian Astronomical Journal*, **189**, 1
- Salo H., et al., 2015, *ApJS*, **219**, 4
- Salpeter E. E., 1955, *ApJ*, **121**, 161
- Sandage A., Bedke J., 1994, *The Carnegie atlas of galaxies, Vols 1, II*. Vol. 638, Carnegie Institution of Washington
- Sandage A., Visvanathan N., 1978a, *ApJ*, **223**, 707
- Sandage A., Visvanathan N., 1978b, *ApJ*, **225**, 742
- Sandage A., Freeman K. C., Stokes N. R., 1970, *ApJ*, **160**, 831
- Sanders D. B., Soifer B. T., Elias J. H., Madore B. F., Matthews K., Neugebauer G., Scoville N. Z., 1988, *ApJ*, **325**, 74
- Savorgnan G. A. D., Graham A. W., 2016, *ApJS*, **222**, 10
- Savorgnan G. A. D., Graham A. W., Marconi A., Sani E., 2016, *ApJ*, **817**, 21
- Schawinski K., et al., 2014, *MNRAS*, **440**, 889
- Schimminovich D., et al., 2007, *ApJS*, **173**, 315
- Schlafly E. F., Finkbeiner D. P., 2011, *ApJ*, **737**, 103
- Schlegel D. J., Finkbeiner D. P., Davis M., 1998, *ApJ*, **500**, 525
- Schmidt M., 1959, *ApJ*, **129**, 243
- Schödel R., et al., 2002, *Nature*, **419**, 694
- Schombert J. M., 2018, *AJ*, **155**, 69
- Schombert J., McGaugh S., 2014, *Publ. Astron. Soc. Australia*, **31**, e036
- Schombert J., McGaugh S., Lelli F., 2019, *MNRAS*, **483**, 1496
- Schombert J., McGaugh S., Lelli F., 2022, *AJ*, **163**, 154
- Schweizer F., Seitzer P., 1988, *ApJ*, **328**, 88
- Schweizer F., Seitzer P., 1992, *AJ*, **104**, 1039
- Scott N., Graham A. W., 2013, *ApJ*, **763**, 76
- Scott N., Graham A. W., Schombert J., 2013, *ApJ*, **768**, 76
- Seigar M. S., James P. A., 1998, *MNRAS*, **299**, 672
- Sharples R. M., Carter D., Hawarden T. G., Longmore A. J., 1983, *MNRAS*, **202**, 37
- Shaya E. J., Tully R. B., 1984, *ApJ*, **281**, 56
- Sheth K., et al., 2010, *PASP*, **122**, 1397
- Sil'chenko O., 2013, *Memorie della Societa Astronomica Italiana Supplementi*, **25**, 93
- Sil'chenko O. K., Moiseev A. V., Egorov O. V., 2019, *ApJS*, **244**, 6
- Smail I., Kuntschner H., Kodama T., Smith G. P., Packham C., Fruchter A. S., Hook R. N., 2001, *MNRAS*, **323**, 839
- Smith R. J., 2020, *ARA&A*, **58**, 577
- Smith Castelli A. V., González N. M., Faifer F. R., Forte J. C., 2013, *ApJ*, **772**, 68
- Soria R., et al., 2022, *MNRAS*, **512**, 3284
- Spavone M., 2016, in Napolitano N. R., Longo G., Marconi M., Paolillo M., Iodice E., eds, *Astrophysics and Space Science Proceedings Vol. 42, The Universe of Digital Sky Surveys*. p. 165 ([arXiv:1507.00911](https://arxiv.org/abs/1507.00911)), doi:10.1007/978-3-319-19330-4_26
- Spiniello C., Trager S., Koopmans L. V. E., Conroy C., 2014, *MNRAS*, **438**, 1483
- Spitzer L. J., Baade W., 1951, *ApJ*, **113**, 413
- Strateva I., et al., 2001, *AJ*, **122**, 1861
- Stringer M. J., Benson A. J., 2007, *MNRAS*, **382**, 641
- Swedenborg E., 1734, *Principia rerum naturalium sive novorum tantaminium phenomena mundi elementaris philosophice explicandi*. Friedrich Hekel, Dresden and Leipzig
- Tan J. C., Beltrán M. T., Caselli P., Fontani F., Fuente A., Krumholz M. R., McKee C. F., Stolte A., 2014, in Beuther H., Klessen R. S., Dullemond C. P., Henning T., eds, *Protostars and Planets VI*. pp 149–172 ([arXiv:1402.0919](https://arxiv.org/abs/1402.0919)), doi:10.2458/azu_uapress_9780816531240-ch007
- Tanaka Y., et al., 1995, *Nature*, **375**, 659
- Tanaka M., Goto T., Okamura S., Shimasaku K., Brinkmann J., 2004, *AJ*, **128**, 2677
- Tantalo R., Chiosi C., Bressan A., 1998, *A&A*, **333**, 419
- Tanvir T. S., Krumholz M. R., 2023, *MNRAS*,
- Terrazas B. A., Bell E. F., Henriques B. M. B., White S. D. M., Cattaneo A., Woo J., 2016, *ApJ*, **830**, L12
- Thilker D. A., et al., 2010, *ApJ*, **714**, L171
- Tift W. G., 1969, *AJ*, **74**, 354
- Tisserand P., et al., 2007, *A&A*, **469**, 387
- Toloba E., et al., 2009, *ApJ*, **707**, L17
- Tomita A., Aoki K., Watanabe M., Takata T., Ichikawa S.-i., 2000, *AJ*, **120**, 123
- Toomre A., 1977, *ARA&A*, **15**, 437
- Toomre A., Toomre J., 1972, *ApJ*, **178**, 623
- Tremonti C. A., et al., 2004, *ApJ*, **613**, 898
- Tsukui T., Iguchi S., 2021, *Science*, **372**, 1201
- Urich L., et al., 2017, *A&A*, **606**, A135
- Vika M., Bamford S. P., Häußler B., Rojas A. L., 2014, *MNRAS*, **444**, 3603
- Visvanathan N., Sandage A., 1977, *ApJ*, **216**, 214
- Vollmer B., Marcelin M., Amram P., Balkowski C., Cayatte V., Garrido O., 2000, *A&A*, **364**, 532
- Vorontsov-Vel'Yaminov B. A., Arkhipova V. P., 1962, *Morphological catalogue of galaxies*, **C01**, 0
- Vorontsov-Vel'Yaminov B. A., Arkhipova V. P., 1974, *Trudy Gosudarstvennogo Astronomicheskogo Instituta*, **46**, 1
- Voyer E. N., et al., 2014, *A&A*, **569**, A124
- Wegner G., Grogin N. A., 2008, *AJ*, **136**, 1

- Werner M. W., et al., 2004, *ApJS*, 154, 1
 Whitmore B. C., Schweizer F., 1995, *AJ*, 109, 960
 Worthey G., Faber S. M., Gonzalez J. J., 1992, *ApJ*, 398, 69
 Wright G. S., James P. A., Joseph R. D., McLean I. S., 1990, *Nature*, 344, 417
 Wright E. L., et al., 2010, *AJ*, 140, 1868
 Wright R. J., Lagos C. d. P., Davies L. J. M., Power C., Trayford J. W., Wong O. I., 2019, *MNRAS*, 487, 3740
 Wyder T. K., et al., 2007, *ApJS*, 173, 293
 Yi S. K., et al., 2005, *ApJ*, 619, L111
 Yoon Y., Lim G., 2020, *ApJ*, 905, 154
 York D. G., et al., 2000, *AJ*, 120, 1579
 Young L. M., 2002, *AJ*, 124, 788
 Yuan T., et al., 2017, *ApJ*, 850, 61
 Zavala J., Okamoto T., Frenk C. S., 2008, *MNRAS*, 387, 364
 Zel'dovich Y. B., 1976, *Pisma v Zhurnal Eksperimentalnoi i Teoreticheskoi Fiziki*, 24, 29
 de Jong R. S., 1996, *A&AS*, 118, 557
 de Vaucouleurs G., 1959, *Handbuch der Physik*, 53, 275
 de Vaucouleurs G., 1961, *ApJS*, 5, 233
 de Vaucouleurs G., Ables H. D., 1968, *ApJ*, 151, 105
 de Vaucouleurs G., de Vaucouleurs A., 1972, *Mem. RAS*, 77, 1
 de Vaucouleurs G., de Vaucouleurs A., Corwin Herold G. J., Buta R. J., Paturel G., Fouque P., 1991, *Third Reference Catalogue of Bright Galaxies*. Springer, New York
 di Serego Alighieri S., et al., 2013, *A&A*, 552, A8
 van Dokkum P. G., Franx M., 2001, *ApJ*, 553, 90
 van den Bergh S., 1976, *ApJ*, 206, 883
 van den Bergh S., 1990, *ApJ*, 348, 57
 van den Bergh S., 1997, *AJ*, 113, 2054

APPENDIX A: BULGE-TO-DISC FLUX RATIOS

Use of the corrective formula (Eq. 6) for dust and inclination, collectively referred to as attenuation, requires observed (pre-corrected) passband-specific B/T flux ratios. The typical differences between these ratios in various passbands are estimated here.

Due to the higher concentration of dust in the centres of galaxies (e.g., di Serego Alighieri et al. 2013; Rathore et al. 2022), the fractional correction for missing bulge light is greater than that for missing disc light (e.g., Driver et al. 2008, their figure 1). The young stellar population in the discs of late-type S galaxies also acts to boost their disc flux and further lower their B/T ratio at bluer wavelengths. However, given that late-type S galaxies (Sc-Sm) have small near-IR B/T ratios < 0.1 , the size of the attenuation correction to the galaxy light remains rather insensitive to the B/T ratio in Eq. 6. On the other hand, for massive S0 galaxies and early-type S galaxies (Sa-Sab), the average near-IR B/T ratio can reach ~ 0.2 to ~ 0.3 (figure 4 in Graham & Sahu 2023a; Graham & Worley 2008, where $B/D \approx 1/4$ to $1/2$). As such, the B/T term in Eq. 6 primarily affects these galaxies.

Fig. A1 displays the mean observed B/T flux ratios of galaxies before application of the attenuation correction from Eq. 6. The data pertain to the samples presented in Graham & Worley (2008), consisting of 186, 193, 114, and 408 data points in the B , R , I , and K -band, respectively. The S0 galaxies are predominantly massive S0 galaxies with $B/T \gtrsim 0.1$ – 0.15 . That is, they are not the low-mass dust-poor S0 galaxies. Aside from the apparently deviant I and K -band entries for the Sab ($T=2$) galaxies, the difference in the B/T ratios are smaller in the early-type disc galaxies. This meshes well with the observation that the colours of (the dust-free portions of) bulges and discs in early-type galaxies are not too dissimilar from each other (Peletier & Balcells 1996). For the late-type spirals, the B/T ratios in the I , R , and B bands are roughly 0.7, 0.5 and 0.25

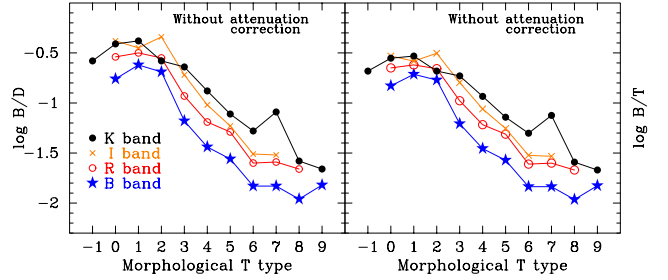


Figure A1. Median bulge-to-disc (left) and bulge-to-total (right) flux ratios in different passbands as a function of galaxy morphological T-type, such that the massive (likely merger-built and dust-rich) S0 galaxies have $T = -1$ & 0, Sa=1, Sb=3, Sc=5, Sd=7, and Sm=9. Figure adapted from Graham & Worley (2008, their figure 7) after removing the attenuation correction from Driver et al. (2008) that accounted for dust and inclination.

times the value in the K -band. For the galaxies with big bulges (S0–Sab), these numbers are taken to be 1.0, 0.8 and 0.5.

This paper has been typeset from a \LaTeX file prepared by the author.